PAPER

Check for updates

Pyrolysis of orange peel waste to pyrofuels and pyrochar: optimization and techno-economic insights for industrial scale-up

Uma Sankar Behera,[a] Sourav Poddar*[b] and Hun-Soo Byun (ID) *[a]

Biomass presents a sustainable alternative to fossil fuels; however, it faces limitations such as high moisture content, low bulk density, and poor grindability. This study investigates the pyrolysis of waste orange peels to produce pyro-char, pyro-oil, and pyro-gas, a process that has been rarely reported in the literature. The effects of pyrolysis temperature, feedstock mass, and heating rate on the yield of these pyro-products were systematically investigated. The biomass was characterized using proximate analysis and thermogravimetric analysis (TGA), while the pyro-products were analyzed for their higher heating value (HHV), lower heating value (LHV), morphology and elemental composition *via* scanning electron microscopy with energy-dispersive X-ray spectroscopy (SEM-EDX), and chemical composition using gas chromatography mass spectrometry (GC-MS). Critical parameters influencing the pyrolysis outcomes were identified: feedstock mass (1–3 kg), temperature (573–1173 K), and heating rate (10–30 K min^{-1}). Under optimal conditions of 2 kg feedstock mass, 873 K temperature, and a heating rate of 20 K min^{-1}, the theoretical yields were 26.52 wt% pyro-char, 22.76 wt% pyro-oil, and 50.72 wt% pyro-gas, with an overall process desirability of approximately 0.7. Experimental yields showed slight deviations, resulting in 28.12 wt% pyro-char, 22.89 wt% pyro-oil, and 48.99 wt% pyro-gas, all within a ±5.7% margin of the theoretical values. The estimated payback period for the initial investment is 1.3 years at a 10% discount rate, which is considerably shorter than the previously reported 6-year period for pyro-gas and pyro-oil production. Scale-up to larger plants is expected to further reduce this duration. This study bridges the gap in comprehensive techno-economic analyses of industrial-scale waste orange peel pyrolysis by producing pyro-char, pyro-oil, and pyro-gas, a three-product yield not previously reported. It offers a sustainable approach to valorizing orange peel waste into high-value products, aligning with Industry 5.0 principles and the United Nations 2030 Sustainable Development Goals.

Sustainability spotlight

Valorising orange peel waste through pyrolysis: advancing the circular economy and energy sustainability in alignment with SDG7, SDG12, and SDG13. Agricultural biomass like orange peel waste presents a promising sustainable alternative to fossil fuels but is often underutilized. This study addresses the critical data and implementation gaps by systematically analyzing the pyrolysis of orange peel waste for the simultaneous production of pyro-char, pyro-oil, and pyro-gas, an integrated tri-product approach not previously reported. Through combined thermochemical analysis and economic modeling, the study demonstrates a payback period of only 1.3 years, substantially improving the feasibility of bioresource valorization at scale. By coupling material recovery with energy generation, the study contributes directly to SDG7 (Affordable and Clean Energy), SDG12 (Responsible Consumption and Production), and SDG13 (Climate Action). It highlights the potential of waste-to-resource strategies to support industrial symbiosis and clean energy transitions, particularly in emerging economies.

1. Introduction

Rapid industrialization and population growth have significantly increased global energy demand, necessitating

[a]Department of Chemical and Biomolecular Engineering, Chonnam National University, Yeosu, Jeonnam 59626, S. Korea. E-mail: hsbyun@jnu.ac.kr; Fax: +82-61-659-7299; Tel: +82-61-659-7296

[b]Department of Chemical Engineering, Haldia Institute of Technology, Haldia, West Bengal-721657, India. E-mail: souravpoddarsxc@gmail.com

sustainable alternative energy sources to mitigate the environmental impacts associated with fossil fuel consumption.[1] Currently, fossil fuels such as coal, natural gas, and petroleum remain the primary energy sources;[2,3] however, their prolonged use leads to serious environmental degradation and long-term sustainability concerns. As a result, there is a growing global transition toward renewable energy sources to reduce dependency on fossil fuels and address these environmental challenges. For instance, orange peel pyrolysis converts agricultural waste into pyro-products (pyro-oil, pyro-char, and pyro-gas) that

directly replace fossil fuel-derived materials while simultaneously reducing methane emissions and petroleum dependency across transportation, manufacturing, and pharmaceutical sectors.

Agro-based biomass has emerged as a promising renewable resource for energy production, offering the potential to bridge the widening supply–demand gap. Among various biomass feedstocks, orange peel waste has gained attention for producing sustainable energy products such as low-ash coke. With global orange production reaching approximately 60 million tons annually, an estimated 32 million tons of orange peel waste are generated, presenting significant environmental and waste management challenges.[4] In countries like India, this biomass is predominantly disposed of in landfills,[5,6] further exacerbating these issues. Orange peels are rich in valuable constituents such as starch, cellulose, fat, lignin, ash, pectin, and flavonoids, making them an ideal feedstock for thermochemical conversion processes.[6] Pyrolysis is a well-established thermal degradation method used to convert biomass into valuable products. This process involves the rapid heating of biomass in an inert atmosphere at temperatures ranging from 473 K to 1273 K,[7] producing three primary products: pyro-char (solid), pyro-oil (liquid), and pyro-gas (gaseous). The yield distribution of these products is highly dependent on processing conditions, particularly temperature. The pyrolysis process is governed by several key reaction mechanisms, including decarboxylation, dehydration, and demethylation. This reaction mechanism influences the formation of pyro-char, pyro-oil, and pyro-gas. Pyro-char, a carbon-rich solid residue, is characterized by a high carbon-to-hydrogen (C/H) ratio and primarily composed of fixed carbon and ash, along with some less volatile hydrocarbons. In

an investigation, Selvarajoo *et al.*[8] reported pyro-char yields ranging from 22% to 53% when citrus peel biomass was pyrolyzed at temperatures between 573 K and 973 K. Similarly, another study demonstrated that approximately 21 to 35 wt% of pyro-char can be obtained from various biomass sources under comparable pyrolysis.[9] Pyro-oil is a dark brown liquid with a smoky odor and primarily consists of oxygenated hydrocarbons, including tars, oils, phenols, and waxes.[10] Shoo *et al.*[10] reported nearly 50% weight loss of biomass at 773 K for particle sizes ranging from 0.6 mm to 0.8 mm, indicating a 50% conversion into various pyrolysis products.[10] Chaiwong *et al.*[11] observed yields of approximately 42% pyro-oil and 33% pyro-char from algae biomass when processed at temperatures between 773 K and 823 K. Amrullah *et al.*[12] reported 30.97% of phenol yield at 773 K from a biomass coconut shell. Another study also reported a nearly 50% increase in pyro-oil production when polyethylene terephthalate was added to the pyrolysis feed.[13] These findings suggest that pyro-char, pyro-oil, and pyro-gas can be produced in relatively comparable proportions, although the exact distribution varies depending on operating conditions. Generally, the pyrolysis process is classified based on the temperature. Different pyrolysis processes based on the temperature and their advantages and disadvantages are provided in Table 1.

The pyrolysis process depends on parameters such as the heating rate, temperature, residence time, and operational mode (batch or continuous).[14,15] The composition and yield distribution of pyrolysis products are significantly influenced by factors including biomass type, reactor configuration, temperature, feedstock and heating rate. Optimizing parameters such as temperature, feedstock and heating rate is essential to achieve a desirable balance among char, oil, and gas yields.[16–18]

Table 1 Summary of different types of pyrolysis based on temperature and their advantages and disadvantages

Pyrolysis type	Temperature (°C)	Heating rate (°C s⁻¹)	Advantages	Disadvantages	References
Slow	300–700	Low (0.1–1)	• Simple setup • Suitable for producing stable pyro-char • High char yield	• Longer residence time • Low liquid fuel yield • Less efficiency	19–21
Fast	450–700	High (∼200)	• High oil yield • Short residence time (<5 s) • Suitable for pyro oil production	• Need rapid heating and cooling • Complex reactor design • Bio-oil is often acidic	22–24
Flash	600–1000	Very high (1000–2500)	• Maximum oil yield • Very short residence time • Efficient for specific chemicals	• High energy input • Technical challenges • Need small particle size	25
Intermediate	400–550	Moderate (1–10)	• Nearly equal formation of char and oil • Flexible operation • Operational flexibility and lower capital cost	• May not optimize for a single product • Advance control conditions	26
Vacuum	300–600	Low to moderate	• Improve pyro oil quality • Reduces secondary reactions	• Requires a vacuum system • Lower gas yield • Increases cost and complexity	27
Multi-stage pyrolysis	300–900	Low to moderate	• Drying of biomass (30–150 °C) • Devolatilization of biomass (200 – 600 °C) • Char formation/Gasification stage (700 – 900 °C)	• To optimize product yield • Quality of the product • Energy consumption • Flexibility and control	28–30

Understanding the relationships between these key variables is critical for enhancing process efficiency and maximizing product yield. Various optimization techniques have been employed to evaluate the interdependence among process parameters. Among these, response surface methodology (RSM) is widely recognized as an effective statistical approach for process optimization. RSM employs experimental designs such as the Plackett–Burman design, Box–Behnken design, the Doehlert matrix, and central composite design to systematically assess and optimize process variables.[31] Recent studies[32–36] have demonstrated the efficacy of RSM in optimizing pyrolysis yields from biomass, confirming its suitability for advanced process optimization.

Economic analysis plays a crucial role in process design by providing reliable estimates of capital investment and operating costs. These early-stage evaluations are essential for determining total investment and energy consumption, facilitating the scale-up of laboratory processes to industrial applications.[37–40] Assessing feasibility, profitability, and investment risk enables the estimation of production costs for value-added products derived from orange peels. Therefore, evaluating the economic performance including initial investment, operational cost, return on investment (ROI), net present value (NPV), and payback period is critical for determining the commercial viability of the process. Most previous studies[8,41,42] have primarily focused on the production of a single pyrolysis product, with very few investigations addressing the simultaneous generation of two or three major products, *i.e.*, char, oil and gas.[9] This highlights the limited availability of data necessary for scaling up the process to achieve maximum product yields and ensure economic viability. Moreover, a comprehensive techno-economic assessment of industrial-scale pyrolysis of orange peel waste remains largely unaddressed, indicating a significant gap in the practical implementation of such valorization approaches.

This study investigates the pyrolysis of orange peel waste for the simultaneous production of char, oil, and gas, addressing a previously unexplored aspect of biomass valorization. The response surface methodology (RSM) optimization technique was employed to enhance the yields of all three pyro-products. Product characterization was conducted using scanning electron microscopy with energy-dispersive X-ray spectroscopy (SEM-EDS) for char, gas chromatography-mass spectrometry (GC-MS) for oil, and gas chromatography (GC) for gas. A comprehensive economic evaluation incorporating net present value (NPV), internal rate of return (IRR), and payback period has been conducted, offering a unique and previously unexplored perspective on the viability of waste orange peels for valuable product processes.[43] Sensitivity analysis was also conducted to assess the impact of variations in operational parameters on the payback period. Beyond waste mitigation, this process supports the development of an integrated biorefinery and presents a novel model for combining waste valorization with sustainable energy and material production.

2. Materials and procedure

2.1. Preparation of feedstock

Oranges typically range from 0.04 m to 0.12 m in diameter[44,45] and are primarily composed of water, with the remaining 13% consisting of minerals, essential oils, lipids, proteins, fibers, organic acids (such as citric and formic acids), pectin, glucosides, and pentosans.[43] The edible portion accounts for approximately 31–51% of the total fruit weight, while the non-
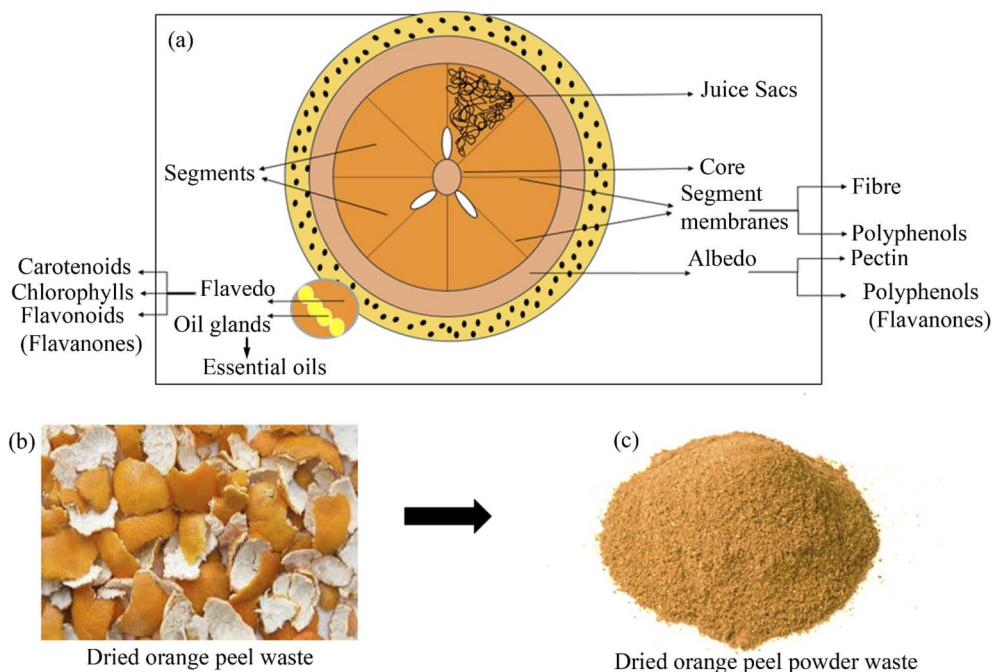

Fig. 1 (a) Anatomic part; (b) dried orange peel waste; (c) powdered form of dried orange peel waste used for pyrolysis.

edible components including segment membranes, albedo, flavedo, core, oil glands, and cuticle make up 49–69% of the total weight.[45,46] This non-edible fraction is referred to as orange peel waste. Fig. 1 provides an overview of the orange components: (a) anatomical parts, (b) dried peels, and (c) powdered peel. 15 kg of orange (mandarin variety) peels were collected from a local market in Haldia, West Bengal, India, for feedstock preparation. The peels were sun-dried for 14 days to reduce moisture content, followed by oven drying at 110 ± 5 °C for approximately 4 h. The dried peels were then ground using a mixer grinder and sieved to achieve a particle size of 0.43 mm. The specific particle size was considered based on the literature study. These processed peels were subsequently used as feedstock in a semi-batch reactor for pyrolysis.

2.2. Experimental setup and procedure

2.2.1 Experimental setup.
The experimental pyrolysis setup is illustrated in Fig. 2. Experiments were conducted in a custom-fabricated cylindrical stainless-steel (SS-314) reactor designed by Purify & Company for laboratory-scale pyrolysis. The reactor has a length of 1.7 m, with internal and external diameters of 0.1195 m and 0.2 m, respectively. It features three openings: a 0.05 m top inlet for material feeding, a 0.04 m bottom outlet for cleaning, and two additional ports connected to B24 pipes—one for nitrogen flow and the other for volatile collection. The reactor is coupled to a 0.8 kW AC heater powered by a three-phase supply and is insulated with glass wool to minimize radiative heat loss. A Ni–Cr thermocouple is installed to monitor the internal temperature. The reactor required approximately 25–113 min to heat up from ambient temperature to the desired pyrolysis temperature (573 K to 1173 K), achieving a heating rate of 8–12° C min^{-1}. After completion of the pyrolysis process, the reactor

was allowed to cool naturally under continuous nitrogen flow for 150–180 min to reach ambient temperature, ensuring complete condensation of volatiles and preventing secondary reactions. These controlled heating and cooling phases were critical for maintaining consistent product yields and preventing thermal degradation of products. The outlet of the reactor is connected to a condenser operating between 8 °C and 12 °C. To maximize pyrolytic oil recovery, the condensable vapors are directed through a bent pipe submerged in a water tank containing water, ice, and salts, maintaining a temperature range of 0 to −2 °C.

2.2.2 Experimental procedure.
A predetermined amount of dried orange peel powder was introduced into the reactor for pyrolysis. Internal reactor surface temperatures were monitored using a Ni–Cr thermocouple (*i.e.*, TC-1, TC-2, and TC-3) connected to a K-type PID controller (see Fig. 2). Nitrogen gas was purged from the bottom of the reactor at a flow rate of 499.8 L h^{-1} to establish an inert atmosphere and facilitate the removal of volatile compounds. The volatiles generated from thermal decomposition were directed through a B24 stainless steel pipe, followed by condensation in a unit maintained at 8–12 °C. A 100 L water tank, equipped with a submersible pump and filled with ice water, was connected to the condenser to enhance the condensation of volatiles into pyrolysis oil. Three condensers were immersed in a salt–ice mixture to maintain a temperature range of 0–2 °C, thereby maximizing oil recovery. The collected pyrolysis oil was stored in 0.025 L vials for subsequent analysis. After cooling to ambient temperature, the resulting pyrolytic char was collected in plastic packets for further study. The pyrolysis procedure for waste orange peels followed the methodology described in a previous publication.[14] Non-condensable gases were quantified volumetrically *via* downward water displacement in a 1 L measuring cylinder and subsequently

TC-: Thermocouple; l: length

Fig. 2 Experimental setup used for the pyrolysis process.
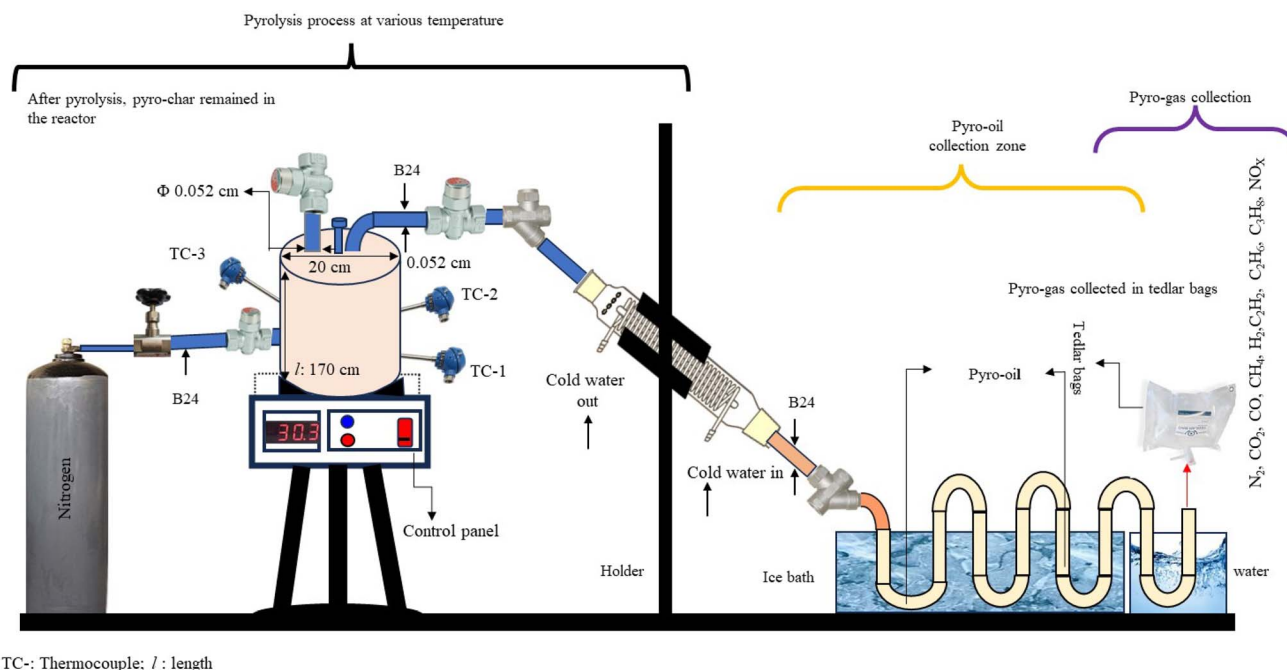
transferred to a 1 L Tedlar bag for compositional analysis. Gas composition was determined using gas chromatography–mass spectrometry (GCMS-TQ8040, Shimadzu, India) to measure the gaseous components' absolute and relative concentrations (wt%). Pyrolysis was performed at temperatures ranging from 573 K to 1173 K under atmospheric pressure (1 atm), and the product distribution was calculated using the equations provided below.

$$(\text{Bio-char) yield\% (wt\%)} = \frac{\text{Weight of solid residue}}{\text{Weight of feed}} \times 100 \quad (1)$$

$$(\text{Bio-oil) yield\% (wt\%)} = \frac{\text{Weight of bio-oil}}{\text{Weight of feed}} \times 100 \quad (2)$$

$$(\text{Bio-gas) yield(wt\%)} = 100 - [(\text{Bio-oil)yield} + (\text{Bio-char)yield}] \quad (3)$$

2.2.3 Operational parameters. Experiments were conducted in four batches to investigate the effect of varying pyrolysis temperatures (573 K to 1173 K) on product yields. Initially, 3 kg of feedstock, sieved to a particle size of 0.43 mm, was loaded into a pyrolyzer. Nitrogen gas was then purged at a flow rate of 499.8 L h^{-1} for 90 min to ensure an oxygen-free environment. Subsequently, the reactor was heated to target temperatures of 573 K, 673 K, 773 K, 873 K, 973 K, 1073 K, and 1173 K. For each experimental run, a specific heating rate between 10 and 30 K min^{-1} was selected. The reactor was heated at the chosen rate until the desired target temperature was reached and then continued to be heated at the same temperature for 60 min. An additional 15 min holding period was employed to ensure complete thermal decomposition of the feedstock. Completion of pyrolysis was indicated by the absence of vapor generation in the water displacement apparatus. The optimal operating condition was identified as the temperature and heating rate combination that yielded the maximum amount of pyrolysis oil.

2.2.4 Mass loss and product separation. Mass loss during the pyrolysis experiments was determined using a high-precision weighing balance before and after each run. The collected pyrolysis oil is a complex mixture of hydrocarbons, water, acid, and alcohol. The viscosity of pyrolysis oil is generally high. To reduce the viscosity and to purify the oil, benzene is added to the pyrolysis oil in the ratio of 10 : 1 (benzene : oil). The mixture was transferred to a 0.25 L separating funnel and left to stand overnight (8–10 h). This step facilitated more precise separation of the oily phase for further purification. After standing, the lighter oil fraction was recovered through vacuum distillation for subsequent characterization.

2.2.5 Evaluation of moisture, volatile ash, and fixed carbon. The moisture content, volatile matter, ash, and fixed carbon of both the sieved waste orange peel powder and pyrolysis char were determined following ASTM D3172-07a.[47] Elemental composition (C, H, N, S, and O) of the pyrolyzed powder, pyrolysis char, and pyrolysis oil was measured using a CHNS microanalyzer (TruSpec, US). This comprehensive analysis ensures accurate characterization of the feedstock and pyrolysis products, which is critical for evaluating their thermal behavior and potential applications.

2.2.6 Higher heating value (HHV) and the lower heating value (LHV). The HHV and LHV of the pyrolyzed powder (char) were calculated using eqn (4) and (5).[48]

$$\text{LHV(MJ kg}^{-1}) = \frac{0.0041868(1 + 0.15[O])\left(7837.667[C] + 33888.89(H) - \frac{O}{8}\right)}{1000} \quad (4)$$

$$\text{HHV(MJ kg}^{-1}) = \frac{\text{LHV} + 21.97[H]}{1000} \quad (5)$$

Similarly, the HHV and LHV of pyrolysis oil were estimated using eqn (6) and (7).[49,50]

$$\text{LHV(MJ kg}^{-1}) = \text{HHV} - 218.3[H](\text{wt\%}) \quad (6)$$

$$\text{HHV(MJ kg}^{-1}) = 338.2[C] + 1442.8\left(H - \frac{O}{8}\right) \quad (7)$$

The HHV and LHV of the pyrolysis gases were determined using eqn (8) and (9).[51]

$$\text{HHV(MJ Nm}^{-3}) = 12.662X_{CO} + 39.782X_{CH_4} + 12.769X_{H_2} + 58.059X_{C_2H_2} + 69.693X_{C_2H_6} + 101.242X_{C_3H_8} \quad (8)$$

$$\text{LHV(MJ Nm}^{-3}) = 12.662X_{CO} + 35.814X_{CH_4} + 10.788X_{H_2} + 56.078X_{C_2H_2} + 63.748X_{C_2H_6} + 93.215X_{C_3H_8} \quad (9)$$

2.3. Characterization procedure

2.3.1 Proximate and ultimate analysis. The proximate analysis determining moisture, volatile matter, ash, and fixed carbon was conducted on both the feedstock and pyrolysis char according to ASTM D3172-89. As previously noted, ultimate (elemental) analysis of the biomass, pyrolysis char, and pyrolysis oil was carried out using a CHNS microanalyzer (TruSpec, US) to quantify carbon, hydrogen, nitrogen, sulfur, and oxygen contents.

2.3.2 Thermogravimetric analysis (TGA). TGA was performed on about 11–12 mg of biomass using a TGA 400 system (PerkinElmer, USA) to investigate thermal degradation behavior. The samples were thermally decomposed at heating rates of 10 K min^{-1}, 15 K min^{-1}, 20 K min^{-1}, 25 K min^{-1}, and 30 K min^{-1} under a nitrogen atmosphere, maintained at a flow rate of 0.12 L min^{-1}.

2.4. Pyrolysis parameter optimization using design of experiments (DOE)

The operational parameters, including feedstock mass and the heating rate, hold direct relevance for industrial scale-up. Feedstock mass determines the reactor loading, which

Table 2 Process criteria and independent variables considered for pyrolysis of orange peel waste[a]

Symbol	Parameter	Units	Minimum	Maximum	Coded low	Coded high	Mean	Std. dev.
A	Feedstock biomass	kg	1	3	$-1 \leftrightarrow 1$	$+1 \leftrightarrow 3$	2	0.73
B	Temperature	K	573	1173	$-1 \leftrightarrow 573$	$+1 \leftrightarrow 1173$	873	217.64
C	Heating rate	$K\ min^{-1}$	10	30	$-1 \leftrightarrow 10$	$+1 \leftrightarrow 30$	20	7.25

[a] Type: numeric; subtype: continuous.

influences heat and mass transfer efficiency during pyrolysis, while the heating rate governs the rate of thermal decomposition and secondary reactions. In large-scale systems, these parameters translate into practical considerations such as reactor design, energy input requirements, throughput capacity, and overall process stability. Therefore, their systematic evaluation at the laboratory scale provides essential insights for designing scalable and economically viable pyrolysis operations. Table 2 presents the process criteria and independent variables considered for the pyrolysis of orange peel waste. It summarizes the parameters used in the experimental design and highlights the variables adjusted during the optimization study. Fig. S1 (SI) illustrates the schematic representation of the CCD process. This offers a clear visualization of the experimental design framework and the associated optimization workflow.

The current study employed CCD for experimental design and RSM for process optimization to enhance process efficiency and support scale-up.[52] CCD based on the Box–Wilson model estimates curvature by combining factorial, axial, and center points, with the parameter α defining the design space.[53,54] The successful application of CCD requires systematic analysis of experimental data and validation of the model against observed values, with adjustments made if discrepancies arise.[55–57] The total number of experiments in CCD is determined using eqn (10).

$$\omega = \xi^2 + 2\xi + \psi \qquad (10)$$

ω represents the overall number of experiments, ξ represents the number of independent variables investigated, and ψ represents the total number of center point repetitions. A critical aspect of CCD is the calculation of the axial distance (α\alphaα), which defines the position of the star points in the experimental region. The design geometry, whether orthogonal, spherical, rotatable, or face-centered is further characterized using the β value. For balancing spherical and face-centered design properties, β is calculated using eqn (11).

$$\beta = [2^m]^{0.25} \qquad (11)$$

Here, m denotes the number of factors. An axial point is ensured to lie within the factorial region when the beta (β) value equals 1, which is the desired configuration in CCD. The relationship between the response and the independent variables is modeled using a second-order polynomial equation given below :[58]

$$D = E_o + \sum_{i=1}^{k} E_i F_i + \sum_{i=1}^{k} E_{ii} F_{ii}^2 + \sum_{i=1}^{k} \sum_{\neq j=1}^{k} E_{ij} F_i F_j + \xi \qquad (12)$$

In this equation, D represents the response variable, k denotes the total number of independent factors, and E_0 is the intercept. The coefficients i, ii, and ij with E correspond to the linear, quadratic, and interaction effects, respectively. Meanwhile, F_i and F_j represent the coded levels of the independent variables.[59,60]

2.4.1 Optimization employing the desirability function. In addition to the DOE, criteria from the desirability function were employed to optimize the pyrolysis parameters. This method identifies the optimal process conditions by referencing assumed ideal values for target responses, including feedstock biomass, temperature, and heating rate.

Optimization plays a critical role in achieving desirable outcomes and depends on multiple influencing factors. Ensuring consistent reproducibility requires the development and stabilization of the optimization process. Therefore, optimization was conducted by establishing well-defined objectives and benchmarks. The optimization process is governed by the following equation:[59]

$$\eta(x) = \left(\prod_{i=1}^{n} \iota_i^{\kappa_i} \right)^{1/\sum \kappa_i} = (\iota_1^{\kappa_1} \times \iota_2^{\kappa_2} \dots \times \iota_n^{\kappa_n})^{1/\sum \kappa_i} \qquad (13)$$

where ι_i denotes the ideal range for each response, n is the number of response variables evaluated, and $\eta(x)$ represents the target output after assigning individual weights to each response. Each relevant parameter is assigned a measure (κ_i) ranging from 1(+) to 5(++++). To normalize the objective function, all fundamental values are standardized or scaled to a common reference point. The desirability function ranges from 0 to 1, where 0 indicates the least favorable outcome and 1 represents the most optimal result. These values quantify how closely the response approximates the desired target. Prior to batch experiments, the desirability function is utilized to determine the experimental parameters that are most likely to yield optimal production of pyrolysis char, oil, and gas, while minimizing errors.

2.5. Pyrolysis product-characterization technique

The surface morphology of the pyrolysis char was examined using a scanning electron microscope (JSM 5610 LV, JEOL, Japan). Prior to analysis, the adsorbent was sputter-coated with gold–palladium at a wavelength of 600 nm under high vacuum and an accelerating voltage of 20 kV. Images were captured at a magnification of 250× to characterize the sample morphology. Morphological changes in orange peel waste before and after pyrolysis were further analyzed using SEM

equipped with energy-dispersive X-ray spectroscopy (SEM-EDS) capabilities.[12] The GC-MS analysis of the pyrolysis oils was performed using an Agilent 6890 GC coupled with a 5973 MSD and HP-5 column (2.5×10^{-7} m × 30 m × 0.00025 m). The oven was initially held at 343 K for 4 min, ramped to 573 K at a constant rate of 5 K min^{-1}, and maintained at 573 K for 30 min. For the first GC-MS analysis set, ten stock solutions of pyrolysis oil were prepared in acetone; the second set was prepared in dichloromethane. Calibration curve solutions were obtained by diluting the mother solutions in the respective solvents. Following the method reported by Sfetsas et al.,[61] 1×10^{-4} L of pyrolysis oil was homogenized with 0.005 L of HPLC-grade ethyl alcohol, filtered, and injected into the system. A helium carrier gas was introduced at a volumetric flow rate of 1.2×10^{-6} L with a constant column flow rate of 0.002 L min^{-1}. The equipment was calibrated with an ionization energy of 72 eV for component ionization. The ion source temperature was maintained at 475 K, and the interface temperature was maintained at 515 K. The scanning MS range was set from 42 m/z to 802 m/z. Pyrolytic oil components were identified at different retention times using the NIST-2017 library database. Gas chromatography (Varian Model CP-3800 GC, Conquer Scientific, US) was used to determine the chemical composition of pyrolysis gas, following the ASTM E112 procedure.[62] The GC system employed a flame ionization detector (FID) with a split-less capillary inlet. The oven was initially held at 333 K for 7 min, then ramped to 543 K at 20 K min^{-1} and held for an additional 25 min. Detector temperatures were maintained at 433 K to analyze various gas mixtures. The identification of gas components was performed based on retention times using reference data from the NIST database.

2.5.1 Gas chromatography of pyrolysis oil. The composition of the pyrolysis oil was analyzed using GC-MS with an Agilent 6890 system (Agilent Technologies, USA), equipped with an HP-5 column (length: 30 m; inner diameter: 0.25 mm; film thickness: 0.25 μm) and a 5973 mass selective detector (MSD). The oven temperature was initially held at 343 K for 4 min, ramped to 573 K at a rate of 5 K min^{-1}, and maintained at that temperature for 30 min. Stock solutions of pyrolysis oil were prepared in acetone and dichloromethane, and calibration curves were generated by serial dilution. The procedure followed a method previously reported by another research group.[61] A mixture of 0.1 μL of pyrolytic oil and 5 mL of HPLC-grade ethyl alcohol was filtered prior to injection. A 1.2 μL aliquot was then injected into the non-polar column, using helium as the carrier gas at a constant flow rate of 2 mL min^{-1}. The ionization energy was set at 72 eV, with the ion source and interface temperatures maintained at 475 K and 515 K, respectively. Scanning was performed over an m/z range of 42 to 802. Compound identification was carried out using the NIST library database.

2.5.2 Gas chromatography of pyrolytic gas. The chemical composition of pyrolysis gas derived from feedstocks was analyzed using gas chromatography (Varian CP-3800 GC, Conquer Scientific, USA), following the ASTM E112 method. The system was equipped with an FID and a splitless capillary inlet. The oven temperature was held at 333 K for 7 min, then

increased to 543 K at a rate of 20 K min^{-1}, and maintained at 543 K for 25 min. The detector temperature was set at 433 K. Gas components were identified based on retention time using the NIST library as a reference.

2.6. A cost-benefit analysis of orange peel waste

Table S1 (SI) presents the parameters used to estimate the capital and operational expenses of the process plant. The total cost of the plant was calculated using the Peters and Timmerhaus method, which incorporates Lang factors added to the projected delivery costs of major equipment components.[63] This method is widely recognized for its accuracy and is based on an extensive review of 156 capital cost estimates. It was also applied by Goksal[64] and Bi et al..[65] To adjust the equipment, purchase cost (EPC),[66] the Chemical Engineering Plant Cost Index (CEPCI) value of 699 for the year 2022, as reported by Seider et al.,[67] was used. Scaling and installation adjustment factors were applied to align the equipment costs with specific design requirements, such as capacity, volumetric flow rate, and construction material. The estimation of direct and indirect expenses followed the methodologies proposed by Chhabra et al.[68] and Seider et al.[67] The fixed capital investment cost (TCIC) was determined by summing the total plant direct cost (TPDC), total plant indirect cost (TPIC), and contractor and contingency cost (CFC). For the calculation of the overall capital investment, working capital was assumed to be 5% of the total and startup costs were estimated at 10%. The annual operational cost of the plant includes both fixed and variable components. Fixed operational costs comprise recurring expenditures such as wages, maintenance, insurance, taxes, and overheads, while variable operational costs include raw materials, utilities, consumables, and laboratory expenses. The cost of raw materials was determined in accordance with Indian Commission standards for government-regulated prices.[69] For this study, a base quantity of 23 040 kg of feedstock was considered at an annual rate of ₹16 kg^{-1} (i.e., \$0.192 kg^{-1}) in the Indian context. Electricity charges were based on standard industrial rates in India. Additional operational cost parameters were derived from the studies of Shah and Valaki[70] and Fodah et al.[71]

Economic performance indicators used to evaluate the feasibility of pyrolyzing orange peel waste include the payback period (PB), internal rate of return (IRR), and net present value (NPV). The discounted cash flow method described by Gujjala and Won[72] was used for the financial analysis, assuming an IRR of 10%. The NPV was calculated after deducting applicable taxes. Sensitivity analysis was also conducted to assess the impact of variations in operational parameters on the PB.[73]

3. Results and discussion

3.1. Feed characterization

The proximate and ultimate analyses of orange peel waste, along with its HHV, empirical formula, and elemental composition, are summarized in Table 3 and compared with literature values. The moisture content is 9.2 wt%, falling within the

Table 3 Proximate and ultimate analyses of orange peel waste with the HHV, the empirical formula, elemental composition, and comparison with values reported in the present study and the literature

Analysis	Present study	74	75	76	77	78	9
Proximate analysis							
Moisture	9.20	0.71	7.79	12.84	6.40	5.7	9.20
Ash	2.00	3.37	4.85	2.60	4.30	3.02	2.94
Volatile substance	78.30	73.75	70.80	70.51	76.70	74.6	74.79
Fixed carbon	10.50	22.17	36.09	14.05	12.60	16.68	13.07
Ultimate analysis (wt%)							
Carbon	46.42	52.78	48.65	44.51	46.6	47.0	39.71
Hydrogen	8.00	5.67	5.78	5.99	7.20	6.9	6.20
Nitrogen	0.44	0.72	0.75	1.08	2.70	1.3	0.46
Sulfur	0.50	0.11	—	0.22	0.50	0.09	0.60
Chlorine	0.08	—	—	—	—	0.001	—
Oxygen	44.56	44.56	28.75	48.20	43.00	44.71	53.03
HHV($MJ\ kg^{-1}$)	19.87	19.49	13.89	19.02	18.32	19.43	16.83
LHV($MJ\ kg^{-1}$)	18.38	12.65	12.83	13.35	17.65	15.35	15.30
H/C	2.07	1.29	1.43	1.62	1.86	1.76	1.88
N/C	0.00	0.00	0.00	0.00	0.00	0.02	0.00
S/C	0.00	0.00	—	0.00	0.00	0.00	0.00
O/C	0.72	0.63	0.44	0.81	0.69	0.71	1.00
Molecular weight ($g\ mol^{-1}$)	27.70	25.55	23.19	29.59	27.07	27.35	33.67
Empirical formula	$CH_{2.07}O_{0.72}$	$CH_{1.29}O_{0.63}$	$CH_{1.43}O_{0.44}$	$CH_{1.62}O_{0.81}$	$CH_{1.86}O_{0.69}$	$CH_{1.76}O_{0.71}$	$CH_{1.88}O$

acceptable limit of 10 wt%, thereby reducing the need for additional energy input during processing. A high volatile matter content of 78.3 wt% promotes enhanced reactivity and devolatilization during pyrolysis, while a low ash content of 2 wt% indicates minimal operational complications due to residue buildup. The concentrations of CHNS and O are consistent with values reported for other biomass feedstocks. Notably, low nitrogen and sulfur contents suggest reduced formation of NO_X and SO_X emissions, contributing to a more environmentally benign process. The H/C and O/C molar ratios are 2.07 and 0.72, respectively, with the HHV and LHV measured at 19.87 and 18.38 MJ kg^{-1}. The empirical formula, $CH_{2.07}O_{0.72}$, and the corresponding molecular weight of 27.70 g mol^{-1} indicate that the material is well-suited for pyrolysis.

3.2. Effect of parameters on pyro-products

This section examines the influence of process parameters—including operational temperature, heating rate, and feedstock quantity—on the yields of pyrolysis products. The discussion focuses on how these variables individually and synergistically affect the distribution of pyro-char, pyro-oil, and pyro-gas.

3.2.1 Effect of temperature on pyro-product yield. Fig. 3 a presents the variation in pyrolysis product yields—char, oil, and gas—over a 1 h duration. The yield of pyrolysis char decreases progressively with increasing temperature. In contrast, pyrolysis oil yield increases, peaking at 873 K, before subsequently declining at higher temperatures. Meanwhile, pyrolysis gas yield shows a continuous rise with temperature. These observations are consistent with prior findings reported by another research group,[79] which showed similar trends within the temperature range of 573 K to 773 K. Specifically, oil and gas yields increased between 573 K and 673 K,

accompanied by a reduction in char yield. Beyond 673 K, pyrolysis oil yield decreased, while gas and char yields remained relatively constant. In the present study, the increase in oil yield up to 973 K was due to enhanced devolatilization and secondary cracking of biomass, which favors liquid formation. Beyond this point, the oil yield decreased. In contrast, the gas yield kept increasing, as higher temperatures promote secondary cracking, dehydrogenation, and condensable vapors reforming into permanent gases such as CO, CO_2, CH_4, and H_2. Furthermore, higher temperatures may promote tar cracking and polymerization, reducing the amount of stable condensable liquids. This could be the reason for the observed decline in oil yield and increase in gas yield at elevated temperatures. Similarly, Bhattacharjee and Biswas[47] reported that pyrolysis char yield decreases as the temperature increases from 598 K to 898 K. The pyrolysis oil yield initially increases between 598 K and 798 K, but declines with further temperature increase, while the pyrolysis gas yield steadily increases throughout the entire temperature range. As the temperature increases, the HHV and LHV of pyrolysis char increase, whereas those of pyrolysis oil decrease. These variations are attributed to changes in the elemental composition, namely, the relative percentages of carbon, hydrogen, and oxygen. At elevated temperatures, pyro-char formed during the primary pyrolysis stage undergoes secondary reactions, enhancing the production of liquids and gases at the expense of solid char. Conversely, lower temperatures favor higher pyro-char yields. At high temperatures, the energy supplied to the biomass may exceed the bond dissociation energy, facilitating the release of volatile compounds,[17] which escape as gases and result in decreased solid char yield.
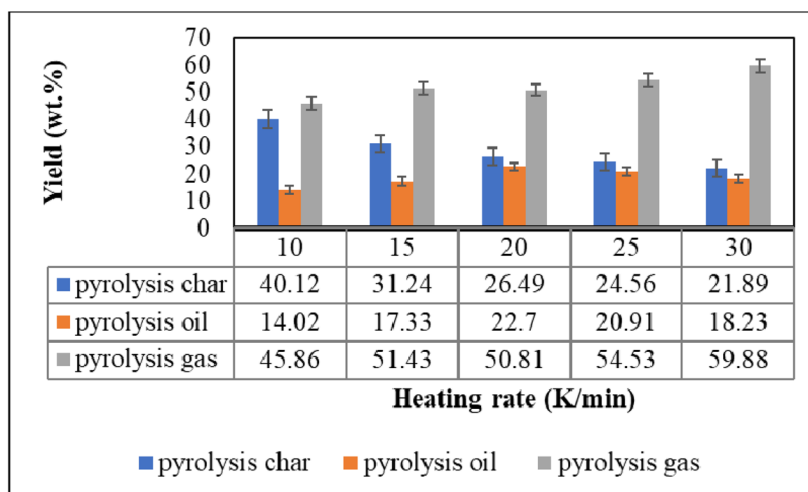
3.2.2 Effect of various heating rates on pyro-product yield. Fig. 3b illustrates the effect of heating rate (K min^{-1}) on the yield of pyrolysis products (wt%). The char yield decreases
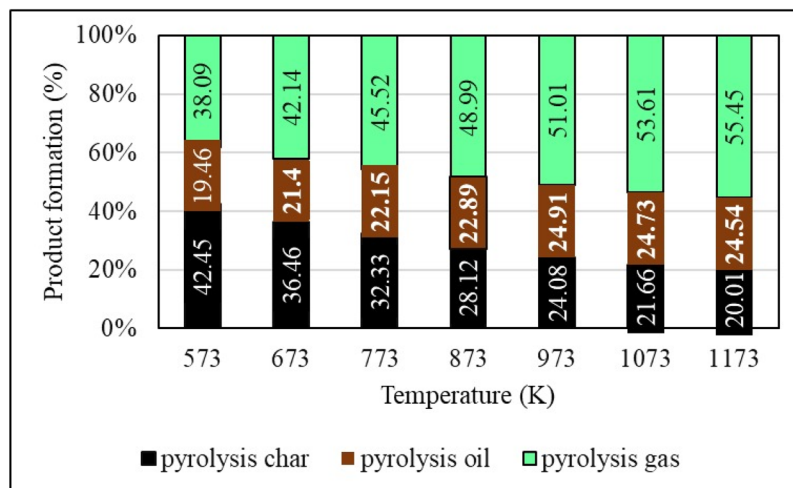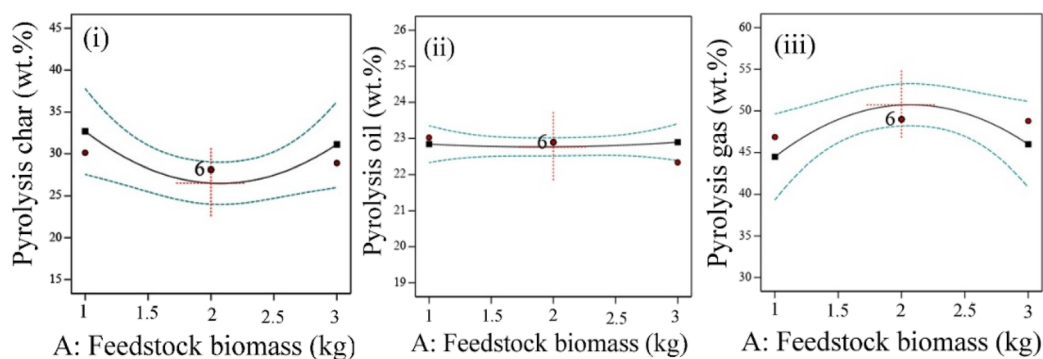
(a)

(b)

(c)

Fig. 3 Effect of process variables on product yield: (a) temperature; (b) heating rate; (c) feedstock mass, with sub-figures (i), (ii), and (iii) representing char, oil, and gas yields, respectively.

consistently as the heating rate increases from 10 K min^{-1} to 30 K min^{-1}. At higher heating rates, biomass decomposes more rapidly into volatile compounds, leading to reduced char formation. This behavior may be attributed to the dominance of secondary pyrolysis reactions under such conditions, which favor greater gas production. The effect of heating rate on char

yield is particularly pronounced at lower temperatures, where these processes are more significant.[17,80]

In contrast, the pyrolysis oil yield increases from 10 K min⁻¹ to 20 K min⁻¹ but subsequently declines as the heating rate increases to 30 K min⁻¹. Meanwhile, the pyrolysis gas yield continues to increase with the rising heating rate. A similar trend in the distribution of pyrolysis products at varying heating rates was reported in other studies,[47] with observed heating rates ranging from 25 K min⁻¹ to 100 K min⁻¹.

3.2.3 Effect of feedstock on pyro-product yield. Fig. 3c illustrates the effect of feedstock biomass mass on the yield of pyrolysis products. Increasing the biomass from 1 kg to 2 kg enhances pyrolysis gas formation from 44 wt% to 50 wt%, likely due to improved thermal decomposition, as the greater biomass volume facilitates more extensive conversion into gaseous products. However, further increasing the biomass to 3 kg results in a decline in gas yield to 47 wt%, which may be attributed to heat transfer limitations within the reactor. At higher biomass loads, uniform heat penetration becomes more challenging, potentially causing incomplete pyrolysis and reduced gas formation. Additionally, increased biomass mass may lead to prolonged residence times, promoting secondary reactions such as char formation, which competes with gas generation and further contributes to the observed decline in gas yield. The production of pyrolysis oil exhibited minimal variation across the biomass range from 1 to 3 kg. Notably, although gas yield increased substantially from 1 to 2 kg, it decreased with a further increase to 3 kg, emphasizing the potential impact of reactor capacity limitations. At higher feedstock volumes, incomplete thermal degradation and uneven heat distribution likely reduce overall gas output. Furthermore, higher biomass inputs may enhance char formation, thereby diminishing gas yields due to competitive product pathways. However, no existing literature is available for a direct comparison of our results regarding the effect of feedstock mass on pyrolysis outcomes, underscoring the uniqueness of our findings in this area.

3.3. Thermogravimetric analysis

Fig. 4 illustrates the thermogravimetric (TG) and derivative thermogravimetry (DTG) analysis of orange peel waste at varying heating rates (10, 20 and 30 K min⁻¹). The pyrolysis process can be delineated into three distinct thermal zones, the temperature ranges of which shift with the increasing heating rate. At 10 K min⁻¹, Zone I spans 303–480 K, Zone II extends from 480–810 K, and Zone III extends from 810–1173 K. For 20 K min⁻¹, the zones are 303–488 K, 488–813 K, and 813–1173 K, respectively. At 30 K min⁻¹, Zone I covers 303–490 K, Zone II extends from 490–815 K, and Zone III extends from 815–1173 K. Zone I primarily involves the removal of moisture and the release of volatile and semi-volatile compounds. This could be the reason why only 12% mass loss was observed in this zone. Orange peels were well dried and the maximum part of the moisture was lost during drying. Zone II corresponds to the thermal degradation of the primary biomass components—cellulose, hemicellulose, and lignin—where the maximum

percentage of mass loss was recorded. In contrast, Zone III exhibited a residual mass loss of approximately 7–8%, primarily attributed to the continued decomposition of lignin and the breakdown of residual char structures. The temperature ranges of these zones broaden with increased heating rates, indicating enhanced thermal inertia and delayed devolatilization. Similarly, Koçer et al.[75] reported three degradation zones at heating rates of 10–40 K min⁻¹, with Zone I occurring below 443 K, Zone II between 443–723 K, and Zone III from 723–873 K. In their study, a lower percentage of biomass decomposition was observed in Zone I at a heating rate of 10 K min⁻¹, whereas higher heating rates (15–30 K min⁻¹) enhanced the conversion efficiency, resulting in 62–76% biomass degradation. The majority of decomposition occurred in Zone II, with Zone III contributing a smaller fraction. The degradation percentages across Zones I, II, and III were approximately 10.31 ± 2.46%, 63.58 ± 1.14%, and 23.63 ± 3.15%, respectively. Zapata et al.[81] also observed similar mass loss patterns during the pyrolysis of orange peel, with 2.73% mass loss up to 273 K, 58.07% between 422–633 K, and 36.09% from 633–858 K. Hemicellulose, cellulose, and lignin—the primary components of biomass—undergo degradation primarily in Zone II, typically between 423–673 K.[82] Hemicellulose, due to its lower molecular weight and thermal stability, degrades at lower temperatures, whereas cellulose, characterized by its extensive hydrogen bonding and crystalline structure, exhibits higher thermal resistance. Lignin, an amorphous, highly cross-linked polymer, demonstrates significant thermal stability and degrades gradually over a broader temperature range.[83] Based on various studies, the thermal degradation temperature ranges for key biomass components are approximately 473–533 K for hemicellulose, 533–633 K for cellulose, and 633–773 K for lignin. According to Abidi et al.,[79] initial mass loss begins at 299 K and continues until 406 K (Zone I), accounting for approximately 12.38% of the total mass loss, primarily due to the evaporation of moisture and light volatile compounds. Zone II, which spans from 407 K to 680 K, is marked by the active pyrolysis stage and accounts for approximately 50.8% of the total mass loss. This stage is characterized by the thermal degradation of pectin, hemicellulose, and cellulose. The maximum degradation temperatures for these components were reported as 435 K for pectin (2.18% mass loss), 503 K for hemicellulose, and 603 K for cellulose (19.08% mass loss).[84] Bensidhom et al.[85] identified distinct decomposition peaks during the pyrolysis of lemon peel at 433 K (9%) for pectin, 508 K (22%) for cellulose, and 601 K (8.3%) for hemicellulose. In Zone III (681–973 K), lignin undergoes slow thermal decomposition, contributing to approximately 4% mass loss at a peak degradation temperature of 735 K. This phase is considered passive pyrolysis, characterized by a relatively low rate of degradation that extends up to 973 K.[86] Additional studies report the thermal degradation ranges of hemicellulose, cellulose, and lignin as 483–598 K, 598–673 K, and 673–1173 K, respectively.[87,88] These findings are consistent with the broader understanding of biomass pyrolysis and offer valuable insight into the thermal behavior of orange peel waste during thermochemical conversion.
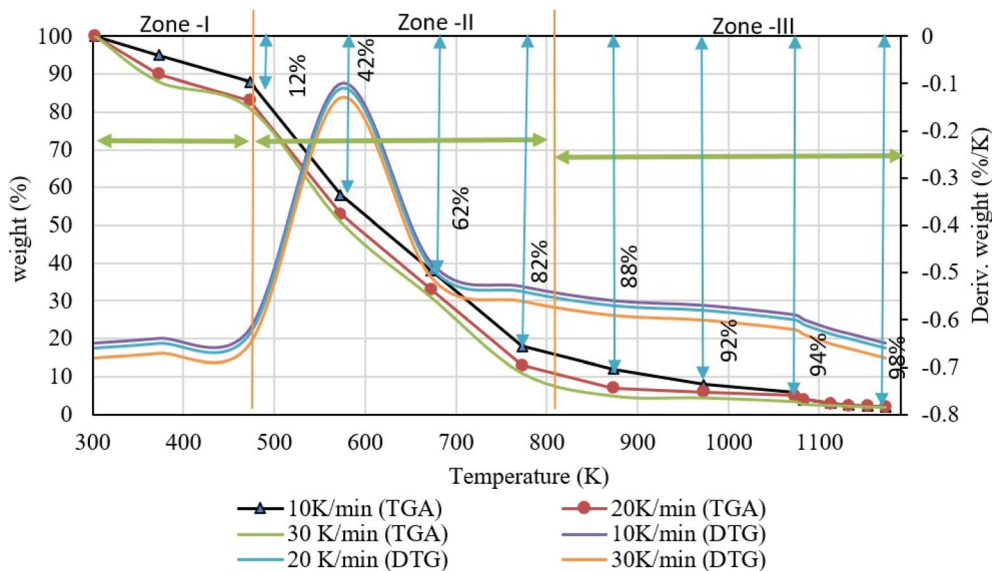
Fig. 4 TGA and DTG analysis curve showing weight loss of orange peel waste at varying heating rates. The TGA curve is the weight loss curve and DTG is the derived weight curve.

3.4. Process scale-up analysis and feasibility evaluation

Evaluating the viability of the pyrolysis process requires a comprehensive analysis of production yield, raw material influence, and production rate. To ensure a realistic assessment and accurate scale-up, the process conversion capability was varied between 0.48 and 0.87. Considering standard engineering assumptions, it is essential to scale up any production process to achieve mass production. For this purpose, the pilot-scale process was extrapolated to an industrial-scale unit using the capacity power law equations.[89,90]

$$\frac{\text{yield}_{p_c}}{\text{yield}_{p_i}} = \left(\frac{\text{Capacity}_2}{\text{Capacity}_1}\right)^m \tag{14}$$

The yield_{p_c} and yield_{p_i} are production yields. The exponent 'm' in this equation represents scaling efficiency. A value of $m = 1$ would indicate perfect linear scaling. However, in practical systems, heat and mass transfer limitations, energy requirements, and equipment design constraints prevent ideal scale-up. For this reason, previous studies have reported realistic values of 'm' between 0.48 and 0.87, where the lower end reflects stronger limitations during scale-up and the higher end indicates better efficiency, though still below ideal conditions. In the present work, this range of 'm' was adopted to model different scenarios and assess feasibility across capacities. The production yield scaling exponent 'm' varies from 0.48 to 0.87, and yield_{p_i}, the initial production yield, was considered at 4 g. The scale-up feasibility was assessed using the defined conversion capabilities and power law, with the scaling exponent m varied between 0.48 and 0.87 to model different scaling scenarios. The process was scaled from a base capacity of 4 g h^{-1} to an industrial throughput of 4000 kg h^{-1}. Fig. 5 illustrates projected product yields at varying process capacities for different scaling factors. This scaling was based on optimal

pyrolysis product yields: pyro-char (0.281), pyro-oil (0.229), and pyro-gas (0.489). The results demonstrated that the production rate increased proportionally with the process capacity, validating the applicability of the power law for this scale-up analysis (see Fig. 5).

3.5. Analysis using statistical methods and development of models

3.5.1 Analysis of the statistical model. Table 4 presents the experimental design for process variables and the corresponding response outputs. The design includes twenty distinct iterations combining various levels of the process variables. The residuals, typically around ±0.79, indicate a close agreement between the predicted and experimental results, while leverage values ranged from 0.11 to 0.79. This section outlines the experimental conditions, focusing on the effects of feedstock biomass, temperature, and heating rate on the pyrolysis product yields. The final process desirability is also discussed. The choice of 2 kg feedstock biomass was made to facilitate process scale-up and to attain optimal operating conditions.

The interactive model terms reveal the combined influence of two parameters, whereas the linear model terms describe the effect of individual parameters. A positive coefficient in the model equation indicates a synergistic effect, while a negative coefficient signifies an antagonistic effect.[91] Table 5 displays the analysis of variance (ANOVA) results, including p-values, F-values, and R^2 coefficients. These values reflect the outcomes of all experimental runs. The proposed model was evaluated using regression model analysis, a validated method for assessing the relationship between response data and model predictions.[92] The p-value quantifies the likelihood of observing deviations due to random chance, while the F-value represents the ratio of variances, indicating model significance. According to the Fischer F-test, a robust and accurate model typically exhibits
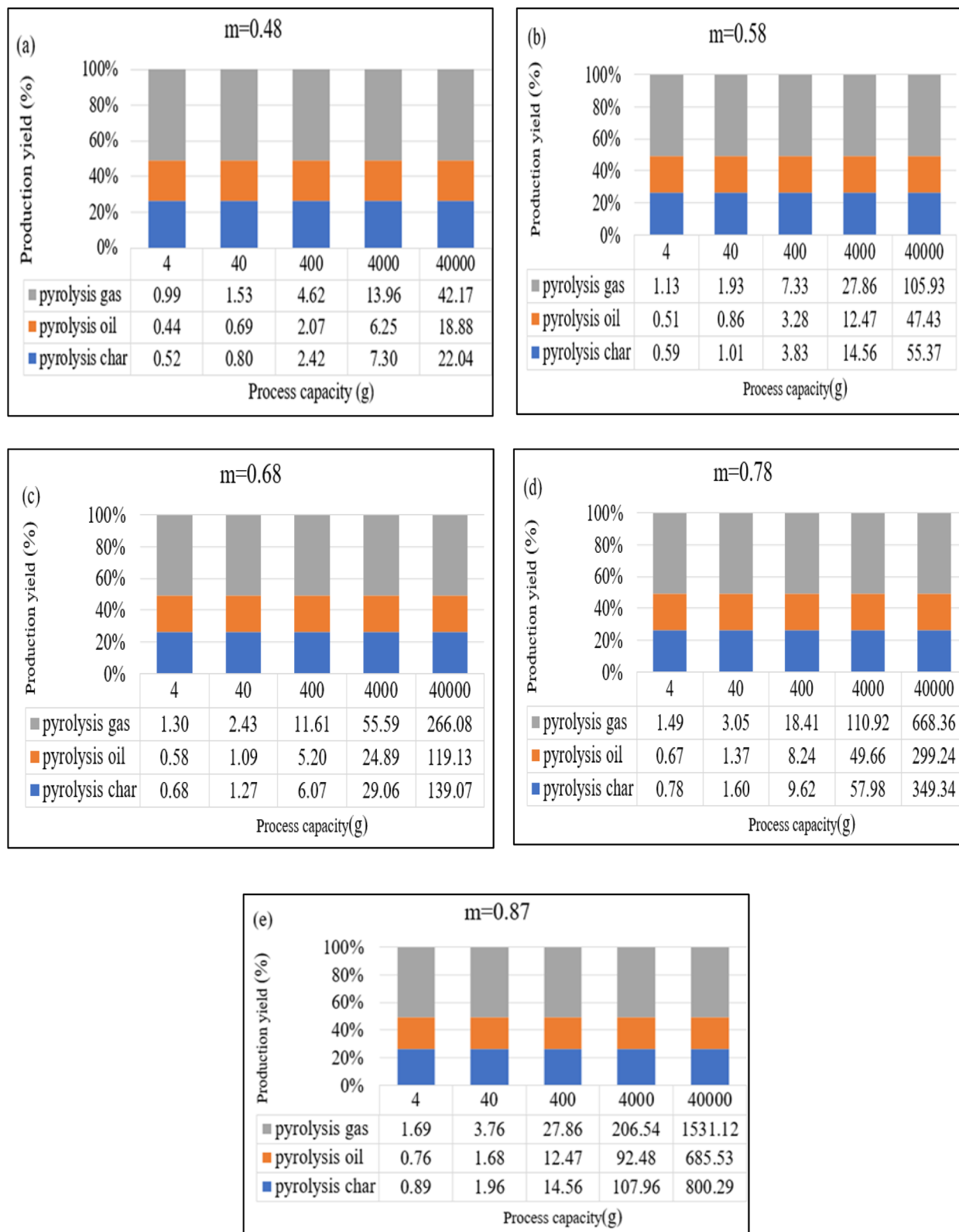
Fig. 5 Projected product yields from orange peel waste pyrolysis at varying process capacities for different scaling factors: (a) $m = 0.48$; (b) $m = 0.58$; (c) $m = 0.68$; (d) $m = 0.78$; (e) $m = 0.87$. Note: m denotes the scaling factor.

low p-values and high F-values.[91,93,94] For pyrolysis char, the ANOVA yielded an F-value of 10.39 and a p-value of 0.05%; for pyrolysis oil, an F-value of 49.41 and a p-value of 0.01% were obtained; and for pyrolysis gas, an F-value of 9.15 and a p-value of 0.09% were obtained. These results confirm the model's efficacy and predictive accuracy. The model was significantly

Table 4 Experimental design involving process variables and corresponding response outputs[a]

Run	Factor A	Factor B	Factor C	Response 1: pyrolysis char (wt%)		Response 2: pyrolysis oil (wt%)		Response 3: pyrolysis gas (wt%)	
				E	T	E	T	E	T
1	1	873	20	30.12	32.69	23.02	22.84	46.86	44.47
2	2	873	30	27.45	34.42	23.06	22.98	49.49	42.60
3	2	873	20	28.12	26.52	22.89	22.76	48.99	50.72
4	2	873	20	28.12	26.52	22.89	22.76	48.99	50.72
5	2	573	20	27.7	30.94	20.21	20.14	52.09	48.92
6	1	1173	30	44.55	42.70	25.33	25.45	30.12	31.85
7	3	873	20	28.89	31.12	22.33	22.89	48.78	45.99
8	1	573	30	40.89	39.17	20.13	20.24	38.98	40.59
9	2	873	20	28.12	26.52	22.89	22.76	48.99	50.72
10	2	873	10	27.89	25.71	22.01	22.47	50.1	51.81
11	1	1173	10	20.56	21.55	24.02	23.86	55.42	54.59
12	3	1173	10	20.01	20.53	24.19	23.99	55.8	55.48
13	2	873	20	28.12	26.52	22.89	22.76	48.99	50.72
14	3	1173	30	42.45	41.24	24.54	24.33	33.01	34.43
15	1	573	10	42.45	42.46	19.46	19.57	38.09	37.96
16	2	873	20	28.12	26.52	22.89	22.76	48.99	50.72
17	3	573	30	39.23	37.04	20.15	20.21	40.62	42.74
18	2	1173	20	21.02	22.58	23.89	24.34	55.09	53.08
19	3	573	10	40.13	40.78	21.01	20.80	38.86	38.42
20	2	873	20	28.12	26.52	22.89	22.76	48.99	50.72

[a] Note: E: experimental; T: theoretical; A: feedstock biomass (kg); B: temperature (K); C: heating rate (K min^{-1}).

Table 5 Analysis of variance (ANOVA) results showing p-values, F-values, and R^2 coefficients[a]

Source	Sum of squares			df	Mean square			F-value			p-value			
	C	O	G		C	O	G	C	O	G	C	O	G	
Model	1004.60	47.78	896.74	9	111.62	5.31	99.64	10.39	49.41	9.15	0.0005	<0.0001	0.0009	Significant
A-feedstock biomass	6.18	0.0068	5.78	1	6.18	0.0068	5.78	0.5751	0.0629	0.5304	0.4657	0.8070	0.4832	
B-temperature	174.81	44.14	43.26	1	174.81	44.14	43.26	16.27	410.82	3.97	0.0024	<0.0001	0.0742	
C-heating rate	189.49	0.6350	212.06	1	189.49	0.6350	212.06	17.64	5.91	19.47	0.0018	0.0354	0.0013	
AB	0.2211	0.5995	0.0924	1	0.2211	0.5995	0.0924	0.0206	5.58	0.0085	0.8888	0.0398	0.9284	
AC	0.0990	0.7750	1.43	1	0.0990	0.7750	1.43	0.0092	7.21	0.1311	0.9254	0.0229	0.7248	
BC	298.78	0.4278	321.82	1	298.78	0.4278	321.82	27.81	3.98	29.55	0.0004	0.0740	0.0003	
A^2	79.62	0.0290	82.69	1	79.62	0.0290	82.69	7.41	0.2701	7.59	0.0215	0.6146	0.0203	
B^2	0.1530	0.7501	0.2255	1	0.1530	0.7501	0.2255	0.0142	6.98	0.0207	0.9074	0.0246	0.8884	
C^2	34.58	0.0038	33.85	1	34.58	0.0038	33.85	3.22	0.0356	3.11	0.1030			
Residual	107.42	1.07	108.91	10	10.74	0.1074	10.89							
Lack of fit	107.42	1.07	108.91	5	21.48	0.2149	21.78							
Pure error	0.0000	0.0000	0.0000	5	0.0000	0.0000	0.0000							
Cor total	1112.03	48.86	1005.65	19										

Fit statistics

Char: Std. Dev.: 3.28; mean: 31.10; C.V.%: 10.54; R^2: 0.90; adjusted R^2: 0.81; predicted R^2: 0.41; Adeq precision: 9.57
Oil: Std. Dev.: 0.33; mean: 22.53; C.V.%: 1.45; R^2: 0.97; adjusted R^2: 0.95; predicted R^2: 0.84; Adeq precision: 25.32
Gas: Std. Dev.: 3.30; mean: 46.36; C.V.%: 7.12; R^2: 0.89; adjusted R^2: 0.79; predicted R^2: 0.37; Adeq precision: 10.12

Model comparison statistics

Char: PRESS: 654.38; −2 log likelihood: 90.38; BIC: 120.34; AICc:134.82
Oil: PRESS: 7.78; −2 log likelihood: −1.72; BIC: 28.24; AICc:42.72
Gas: PRESS: 630.34; −2 log likelihood: 90.65; BIC: 120.61; AICc:135.10

[a] df remains the same for char, oil, and gas; C = pyrolysis char; O = pyrolysis oil; G = pyrolysis gas.

influenced by the quadratic terms A^2 and B^2 ($p < 0.05$), the linear terms A (feedstock mass), B (temperature), and C (heating rate), and the interaction terms AB, AC, and BC. The R^2 coefficient represents the degree of fit between the regression equation and the experimental data, with a value of 1 indicating a perfect fit and 0 indicating no correlation.[58] The model demonstrated strong predictive capability, with R^2 and adjusted R^2 values of 0.81 (pyrolysis char), 0.95 (pyrolysis oil), and 0.79 (pyrolysis gas). The close agreement between adjusted R^2 and predicted R^2—differing by less than 0.4 for pyrolysis char, 0.11 for pyrolysis oil, and 0.42 for pyrolysis gas—further supports the model's reliability and relevance.

$$
\begin{aligned}
\text{Pyrolysis char} = {}& 105.34 - 22.57 \times A - 0.06 \\
& \times B - 2.74 \times C + 5.5 \times 10^{-4} \times A \\
& \times B - 0.01 \times A \times C + 2.04 \times 10^{-3} \\
& \times B \times C + 5.38 \times A^2 + 2.62 \\
& \times 10^{-6} \times B^2 + 0.04 \times C^2
\end{aligned} \tag{15}
$$

$$
\begin{aligned}
\text{Pyrolysis oil} = {}& 10.43 + 1.03 \times A + 0.02 \\
& \times B + 0.04 \times C - 9.13 \times 10^{-4} \times A \\
& \times B - 0.03 \times A \times C + 7.7 \times 10^{-5} \\
& \times B \times C + 0.1 \times A^2 - 5.8 \times 10^{-6} \\
& \times B^2 - 3.73 \times 10^{-4} \times C^2
\end{aligned} \tag{16}
$$

$$
\begin{aligned}
\text{Pyrolysis gas} = {}& -15.79 + 21.54 \times A + 0.04 \\
& \times B + 2.70 \times C + 3.58 \times 10^{-4} \times A \\
& \times B + 0.04 \times A \times B - 2.11 \times 10^{-3} \\
& \times B \times C - 5.48 \times A^2 + 3.18 \times 10^{-6} \\
& \times B^2 - 0.04 \times C^2
\end{aligned} \tag{17}
$$

3.5.2 Process variable interactive impacts. 3D and 2D surface plots were employed to illustrate the interplay among process variables, including feedstock mass, temperature, and heating rate. Fig. 6 presents the combined effects of these factors on the yield of pyrolysis char (wt%). Specifically, Fig. 6a(i) and (ii) display the 2D and 3D surface plots, respectively, of pyrolysis char yield as a function of feedstock mass and temperature. Fig. 6b(i) and (ii) illustrate the yield in relation to feedstock mass and heating rate, while Fig. 6c(i) and (ii) present the yield as a function of temperature and heating rate. According to the ANOVA results, the interaction term in the model exhibited a statistically significant p-value of ≈ 0.0005. The pyrolysis char yield decreased from 42.45% to 20.01% as the feedstock mass increased from 1 to 3 kg and the temperature rose from 573 to 1173 K, indicating a notable interactive effect between these variables. This suggests a favorable correlation between feedstock mass and temperature, with pyrolysis char output being directly proportional to the values of the interactive model parameters—implying that adjusting these parameters upward or downward would yield a corresponding effect. It has been reported that biomass-derived pyrolysis char does not undergo complete carbonization at temperatures below 573 K, regardless of the heating rate. Complete carbonization typically occurs at temperatures ≥ 773 K.[95] An initial increase in both feedstock mass and heating rate led to

a reduction in pyrolysis char yield, reaching a minimum point; however, further increases in these factors resulted in an increase in char production [see Fig. 6b(i) and (ii)]. These findings are consistent with previous studies reporting 28% char yield from sawdust pyrolyzed at 773 K in 60 min residence time[96] and 43% char yield from rice husk pyrolysis at the same temperature in 55 min residence time.[97] Variations in char yield can likely be attributed to differences in feedstock composition, underscoring the importance of selecting appropriate biomass for achieving targeted carbon black yields in specific applications. A detailed examination of the response surfaces reveals that the trends exhibit a falling ridge pattern, characteristic of the polynomial behaviour described in eqn (15) under the framework of RSM. The contour plots exhibit falling ridge patterns [Fig. 6a(i) and 6b(i)] and a simple maximum [Fig. 6c(i)], collectively reflecting the behaviour of a second-order polynomial response.[59,98,99]

Fig. 7 illustrates the combined effects of feedstock mass, temperature, and heating time on pyrolysis oil (wt%) yield. Specifically, Fig. 7a(i) and (ii) display the 2D and 3D surface plots of pyrolysis oil yield as a function of feedstock mass and temperature. Fig. 7b(i) and (ii) show the 2D and 3D surface plots of pyrolysis oil yield as a function of feedstock mass and heating time. Similarly, Fig. 7c(i) and (ii) present the yield as the function of temperature and heating time. According to the ANOVA results, the interactive model term exhibited a highly significant p-value of < 0.0001. The pyrolysis oil yield increased from 19.46% to 24.19% when the feedstock mass was raised from 1 to 3 kg and the temperature increased from 573 to 1173 K, indicating strong positive correlation between these two variables. The yield was directly proportional to the values of the interactive parameters, implying that increasing or decreasing them would result in corresponding changes in oil output. Fig. 7b(i) and (ii) suggest that the response surface becomes steeper as both feedstock mass and heating time increase. Notably, no previous studies have reported this specific behaviour. A detailed examination of the trends in these plots reveals a rising ridge pattern, consistent with the polynomial form described by eqn (16) within the framework of RSM. Furthermore, Fig. 7a(i), b(i) and c(i) each present a monotonic surface, characterized by a smooth, plane-like incline without significant curvature or inflection points, indicative of a second-order polynomial response.[59,99]

Fig. 8 illustrates the combined effects of feedstock mass, temperature, and heating time on pyrolysis gas (wt%) yield. Specifically, Fig. 8a(i) and (ii) present the 2D and 3D surface plots, respectively, of pyrolysis gas yield as a function of feedstock mass and temperature. Fig. 8b(i) and (ii) display the 2D and 3D surface plots as a function of feedstock mass and heating time, while Fig. 8c(i) and (ii) show the corresponding plots for temperature and heating time. The interactive model term exhibited a statistically significant p-value of ≈ 0.0009. The pyrolysis gas yield increased from 38.09% to 55.8% as the feedstock mass was increased from 1 to 3 kg and the temperature was raised from 573 to 1173 K, indicating positive correlation between feedstock mass and temperature with respect to gas production. Fig. 8b(i) and (ii) demonstrate a decreasing
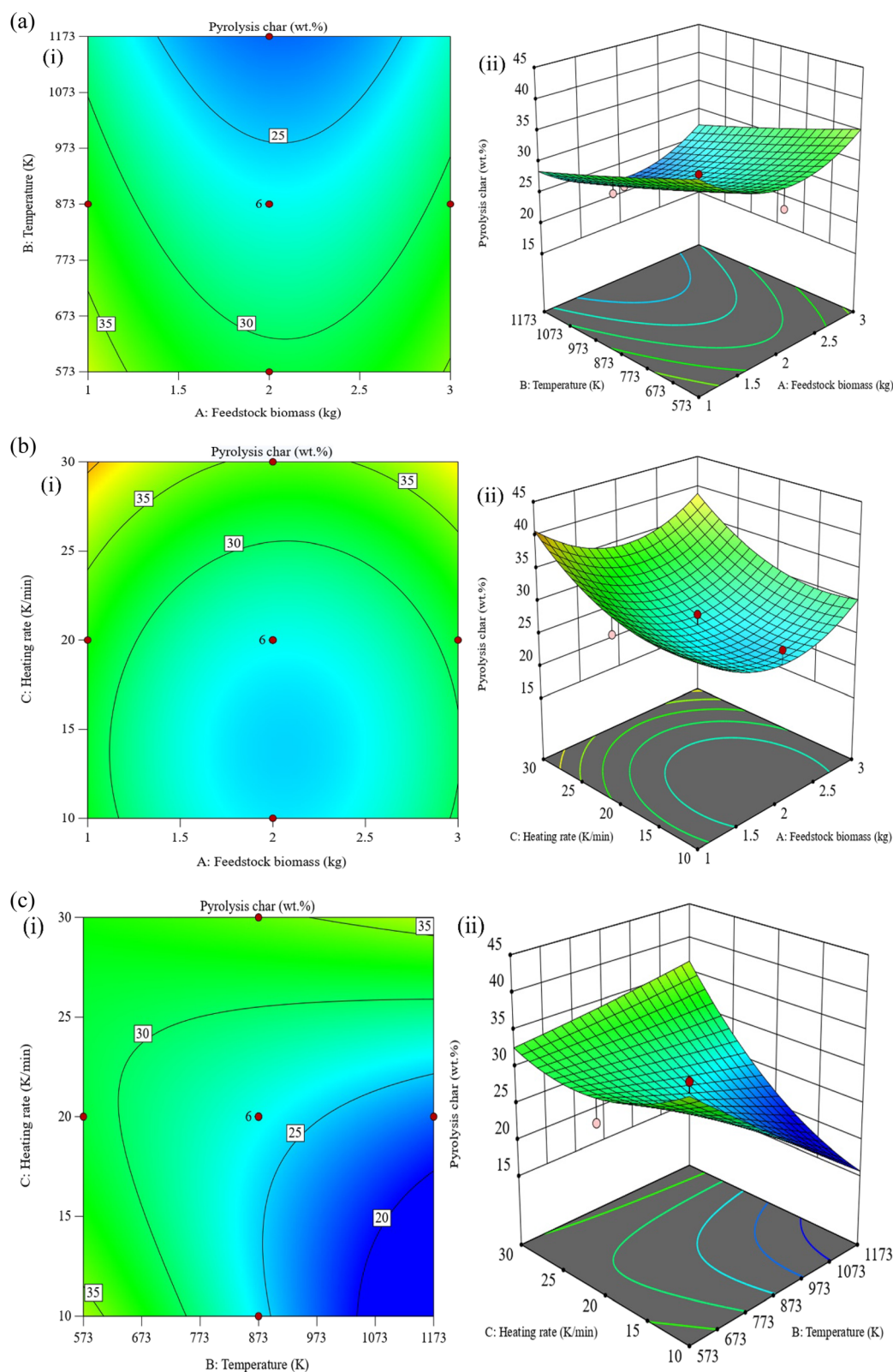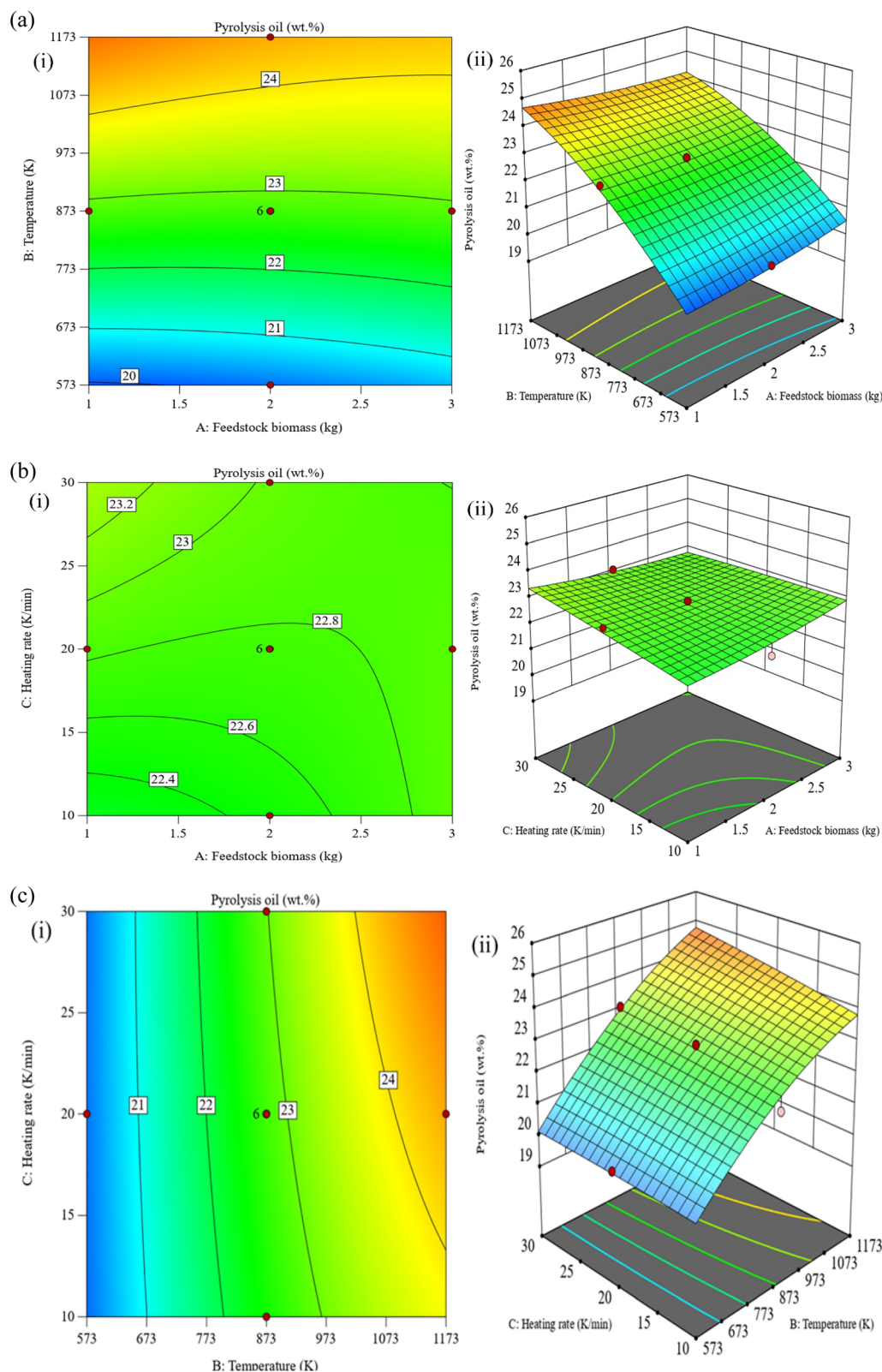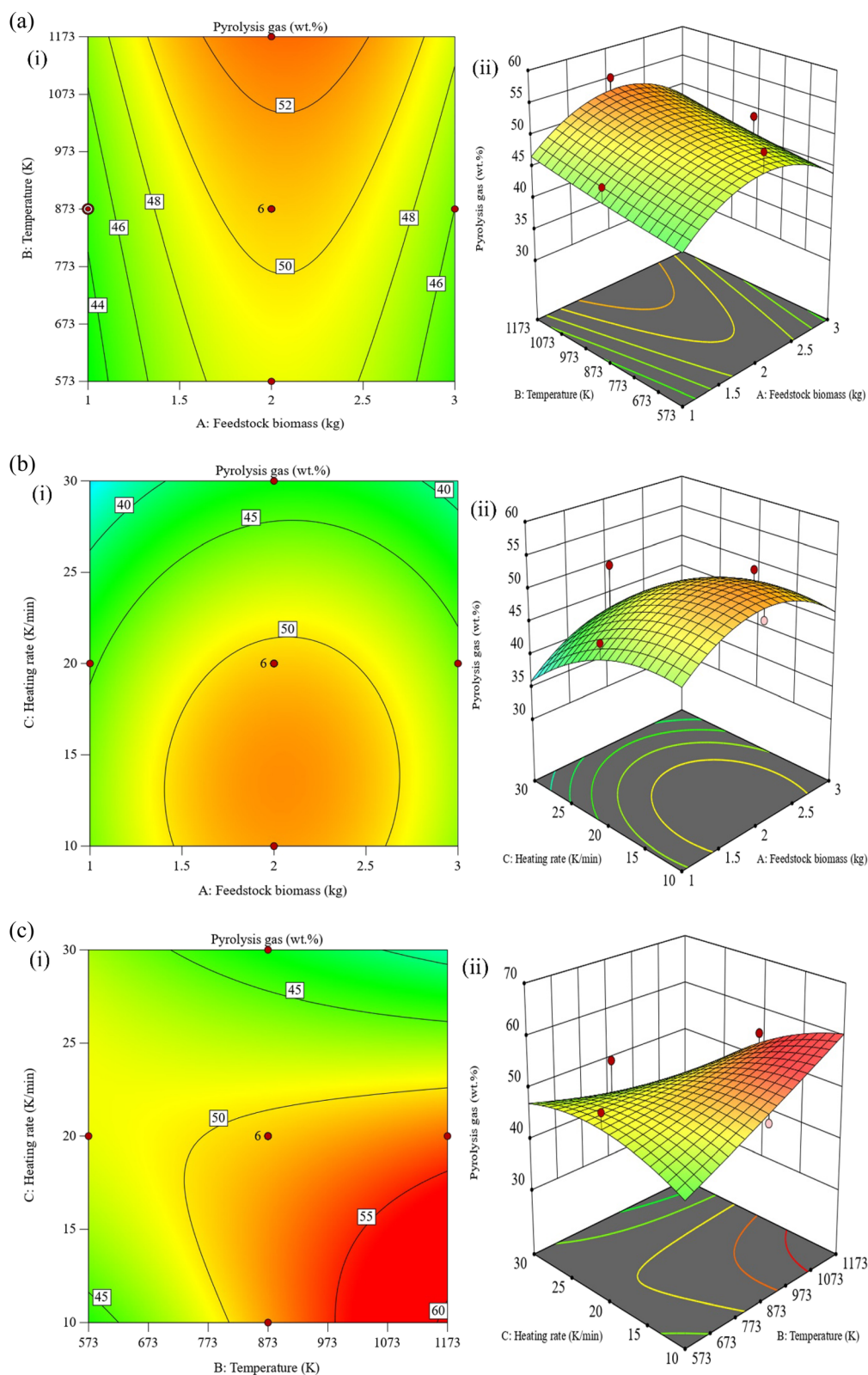
Fig. 6 (a) (i) Two-dimensional contour and (ii) three-dimensional contour plots showing pyrolysis char yield (wt%) as a function of feedstock biomass and temperature. (b) (i) Two-dimensional contour and (ii) three-dimensional contour plots showing pyrolysis char yield (wt%) as a function of feedstock biomass and heating rate. (c) (i) Two-dimensional contour and (ii) three-dimensional contour plots showing pyrolysis char yield (wt%) as a function of heating rate and temperature.

Fig. 7 (a) (i) Two-dimensional contour and (ii) three-dimensional contour plots showing pyrolysis oil yield (wt%) as a function of feedstock biomass and temperature. (b) (i) Two-dimensional contour and (ii) three-dimensional contour plots showing pyrolysis oil yield (wt%) as a function of feedstock biomass and heating rate. (c) (i) Two-dimensional contour and (ii) three-dimensional contour plots showing pyrolysis oil yield (wt%) as a function of heating rate and temperature.

Fig. 8 (a) (i) Two-dimensional contour and (ii) three-dimensional contour plots showing pyrolysis gas yield (wt%) as a function of feedstock biomass and temperature. (b) (i) Two-dimensional contour and (ii) three-dimensional contour plots showing pyrolysis gas yield (wt%) as a function of feedstock biomass and heating rate. (c) (i) Two-dimensional contour and (ii) three-dimensional contour plots showing pyrolysis gas yield (wt%) as a function of heating rate and temperature.

trend in pyrolysis gas yield as feedstock mass and heating time increase. This response pattern was not previously reported in the literature. A detailed analysis of the surface plots reveals that the trends follow a rising ridge pattern, consistent with the polynomial form described in eqn (17) under RSM. Fig. 8a(i) exhibits a rising ridge, Fig. 8b(i) represents a minimax behaviour, and Fig. 8c(i) displays a simple maximum. These surface patterns are characteristic of a second-order polynomial response.[98–100]

3.5.3 Determining ideal process parameters using desirability function methodology.

Several aspects of the pyrolysis experiment and their associated responses were investigated using numerical optimization in Design Expert 13 to determine the optimal batch reaction parameters. The optimization aimed to maximize the values of the previously discussed response variables through a numerical approach based on desirability criteria available within the software—namely, range, minimization/maximization, and target specifications. The desirability function in RSM quantifies how well selected process conditions fulfil multiple optimization goals, with values ranging from 0 (completely undesirable) to 1 (fully desirable). However, the optimization process may require considerable energy and time due to the extensive number of batch experiments needed to obtain reliable results. For all three pyrolysis product yields—char, oil, and gas—numerical optimization was conducted using a CCD within the RSM framework and guided by the desirability function approach.[58] The target values for the process parameters were a feedstock biomass of 2 kg, a temperature of 873 K, and a heating rate of 20 K min^{-1}. Although the design of experiments (DOE) predicted high response values, these conditions were identified as optimal within the constraints of the chosen parameter space. All pyrolysis process variables were assigned the default highest importance level (+++++), indicating a strong influence on the response variables. Each independent and dependent variable was given an equal weight of 1. Table 6a presents the target

constraints for factors and responses, including the optimization goal, lower and upper limits, weights, and assigned importance. Table 6b presents final desirability based on input factors and responses. The optimized solution was obtained at 2 kg feedstock biomass, 873 K temperature, and 20 K min^{-1} heating rate, yielding 26.52 wt% pyrolysis char, 22.76 wt% pyrolysis oil, and 50.72 wt% pyrolysis gas. The final composite desirability value of the process was 0.7. The associated contour plots illustrating the optimization results and minimum standard errors are shown in Fig. 9 (see Fig. 9a–c).

3.6. Pyrolysis char characterization

This section discusses the characteristics of the pyrolysis product yield derived from orange peel waste, obtained under optimized conditions: a feedstock biomass of 2 kg, a pyrolysis temperature of 873 K, and a heating rate of 20 K min^{-1}. The resulting product distribution included 26.52 wt% pyrolysis char, 22.76 wt% pyrolysis oil, and 50.72 wt% pyrolysis gas, with an overall process desirability of 0.70.

3.6.1 CHO and surface morphology of pyrolysis char

3.6.1.1 CHNSO study. The elemental composition, specifically carbon, hydrogen, and oxygen in pyrolysis char, is critical for evaluating its potential as a fuel. An increase in carbon and hydrogen content enhances the heating value of pyro-char, whereas a higher oxygen content reduces it and promotes undesirable reactions such as polymerization. Fig. 10a shows the carbon, hydrogen, and oxygen composition of pyrolysis char produced from orange peel waste. The results indicate that carbon content increases while oxygen content decreases with rising pyrolysis temperature. Hydrogen content also increases with temperature. Nitrogen content declines as the temperature increases, while sulfur content remains relatively unchanged. These findings confirm a more pronounced trend of increasing carbon and decreasing oxygen compared to previous datasets. Similar observations were reported in the literature.[47,101–103] Hernandez-Mena *et al.*[101] observed that pyro-char typically

---

Table 6 Detailed goal specification and the importance of the parameters and optimized conditions of the pyrolysis process along with desirability

(a) Specification of factor goals, upper and lower limits, upper and lower weights, and corresponding importance levels

Name	Goal	Lower limit	Upper limit	Lower weight	Upper weight	Importance
A: Feedstock biomass	In range	1	3	1	5	5
B: Temperature	In range	573	1173	1	5	5
C: Heating rate	In range	10	30	1	5	5
Pyrolysis char	Maximize	20.01	44.55	1	5	5
Pyrolysis oil	Maximize	19.46	25.33	1	5	5
Pyrolysis gas	Maximize	30.12	55.8	1	5	5

(b) Final desirability based on input factors (feedstock biomass, temperature, and heating rate) and responses (pyrolysis char, pyrolysis oil, and pyrolysis gas)

Feedstock biomass (kg)	Temperature (K)	Heating rate (K min^{-1})	pyrolysis char (wt%)	pyrolysis oil (wt%)	pyrolysis gas (wt%)	Desirability
2	873	20	26.52	22.76	50.72	0.70

Fig. 9 (cont.)
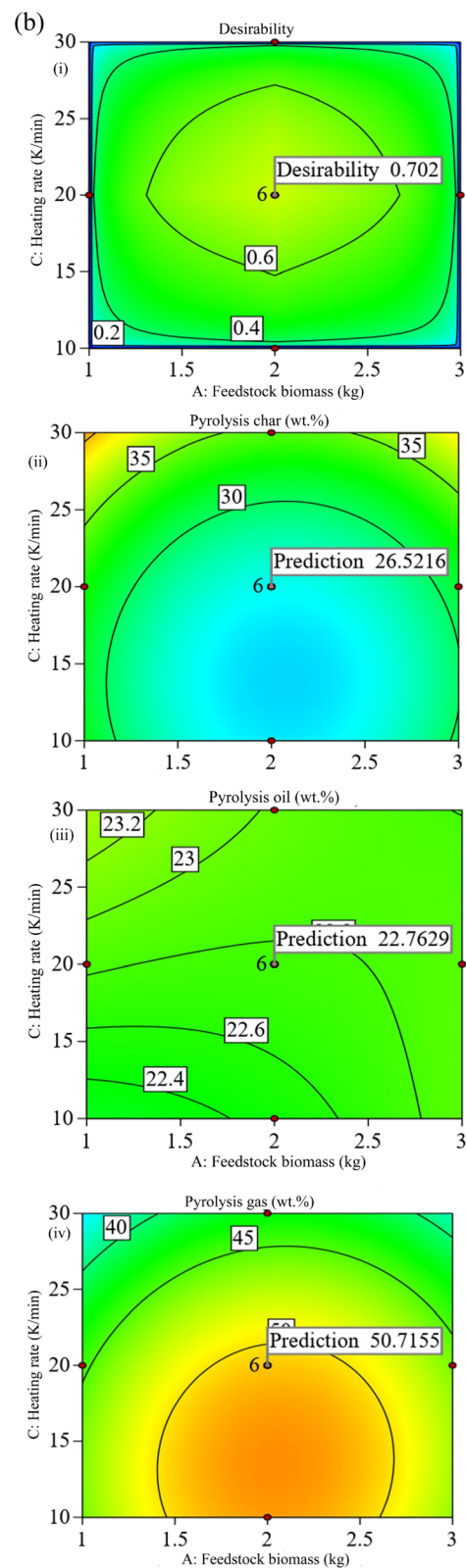
Fig. 9 (cont.)
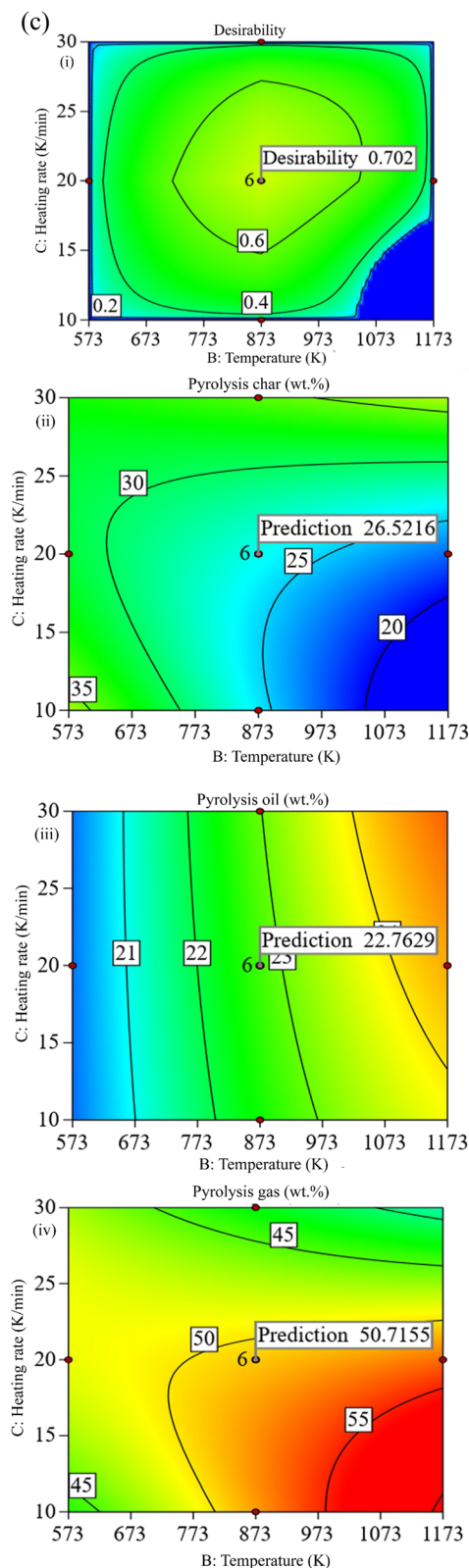
contains low oxygen levels (30–47 wt%) and elevated hydrogen and carbon contents (44–62 wt%), making it suitable for use in gasification or combustion-based energy applications.[103]

3.6.1.2 Scanning electron microscopy with energy-dispersive X-ray spectroscopy (SEM-EDX) analysis. The surface morphology and elemental composition of orange peel waste and its corresponding pyrolysis char were examined using SEM-EDX, as shown in Fig. 10b. The SEM micrographs in Fig. 10b(i) and (ii) reveal a ruptured and spongy surface morphology. The average particle diameter increased from 2.8 μm in the raw biomass to 12.8 μm after pyrolysis, likely due to the breakdown of complex organic structures, the formation of agglomerated compounds, and the volatilization of organic components during pyrolysis. In contrast to the findings of Elnour *et al.*,[104] who reported pyrolysis char with randomly shaped, sharp-edged particles, the pyrolysis char in the present study exhibited a similarly random shape but without sharp edges, featuring deep channels and a more porous structure. The observed morphology, with an average particle size of 12.8 μm, suggests the potential for enhanced mechanical interlocking, as the porous structure could facilitate the infiltration of molten polymer chains.[105,106] Chen *et al.*[107] reported pyrolysis char with sheet-like structures of varying sizes, smooth surfaces, and honeycomb-like voids, noting that auto decomposition occurred at higher temperatures. Their EDX mapping indicated a uniform distribution of elemental components. In the current investigation, energy-dispersive X-ray spectroscopy identified C and O as the major elements, along with impurity Ca, as shown in Fig. 10b(iii). The observations in this study align with those of Kordoghli *et al.*,[108] who reported that high-magnification SEM revealed vibrant surface texture with clearly visible pores in both pyrolysis char and raw biomass samples.

3.6.2 CHO study of pyrolysis-oil using gas chromatography-mass spectrometry (GC-MS). Fig. 11 presents the elemental analysis of pyrolysis oil, highlighting the effects of CHNSO content. With increasing pyrolysis temperature, the oxygen and sulfur content in the pyrolysis oil increases, while the carbon and hydrogen content decreases. These trends are consistent with findings reported by Yang *et al.*[109] in fast pyrolysis. Although that study included catalytic pyrolysis, they noted that carbon content in catalytic pyrolysis oil remained higher than that in non-catalytic oil at temperatures up to 873 K. The present investigation, however, focuses solely on the non-catalytic pyrolysis of orange peel waste. Similar behaviour has been observed in the pyrolysis of other biomass feedstocks, such as paddy husk, within the 723–873 K temperature range.[109,110] The observed increase in oxygen and hydrogen concentrations may be attributed to the loss of carbon through volatilization, resulting in the formation of non-condensable

Fig. 9 (a) Optimization of pyrolysis process parameters [feedstock biomass (kg) and temperature (K)] to maximize char yield using desirability criteria and minimizing standard error: (i) optimized pyrolysis char yield outcome; (ii–iv) optimized conditions for pyrolysis char yield. (b) Optimization of pyrolysis process parameters [feedstock biomass (kg) and heating rate (K min⁻¹)] to maximize oil yield using desirability criteria and minimizing standard error: (i) optimized pyrolysis oil yield outcome; (ii–iv) optimized conditions for pyrolysis oil yield. (c) Optimization of pyrolysis process parameters [temperature (K) and heating rate (K min⁻¹)] to maximize gas yield using desirability criteria and minimizing standard error: (i) optimized pyrolysis gas yield outcome; (ii–iv) optimized conditions for pyrolysis gas yield.

(a)

(b)
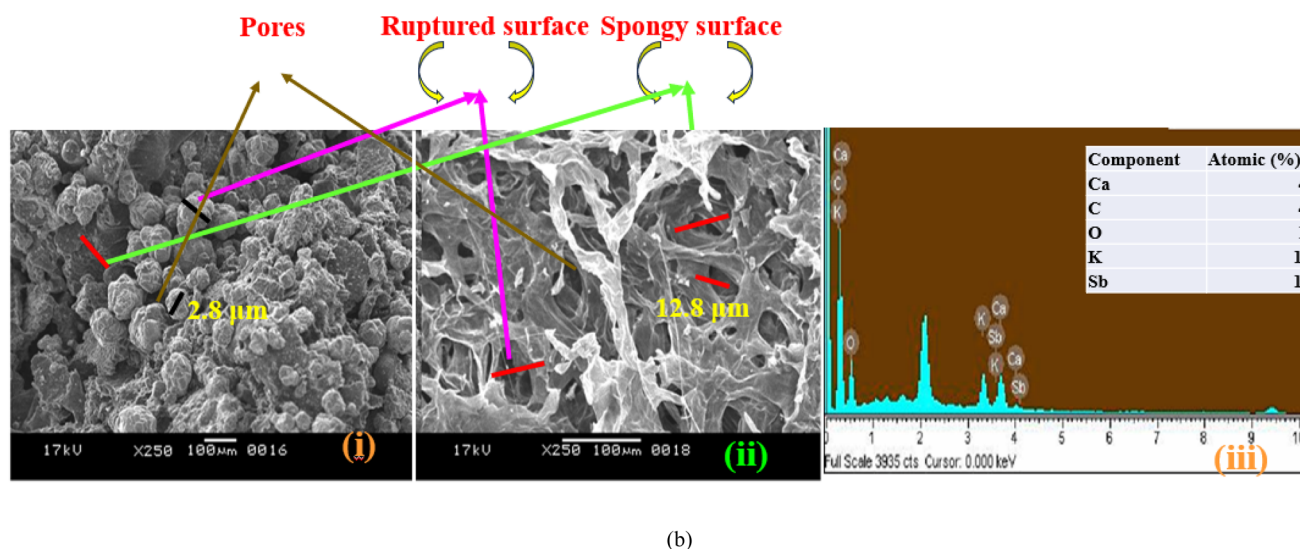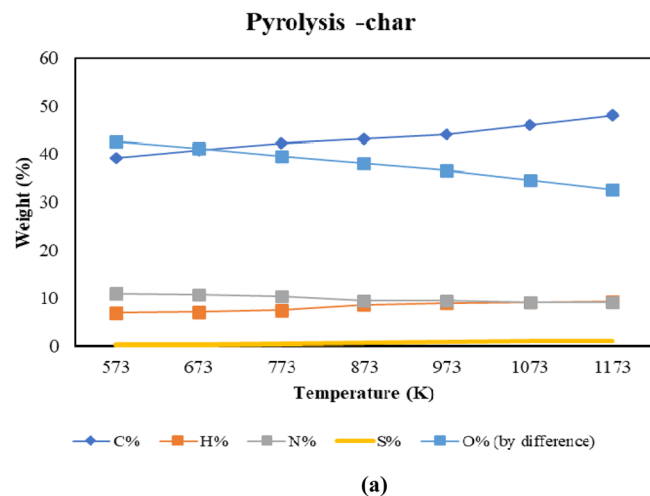
Fig. 10 (a). Effect of CHNSO composition on pyrolysis char; (b) (i) SEM micrograph of orange peel waste; (ii) SEM micrograph of pyrolyzed orange peel waste; (iii) EDX spectrum of pyrolyzed orange peel waste.
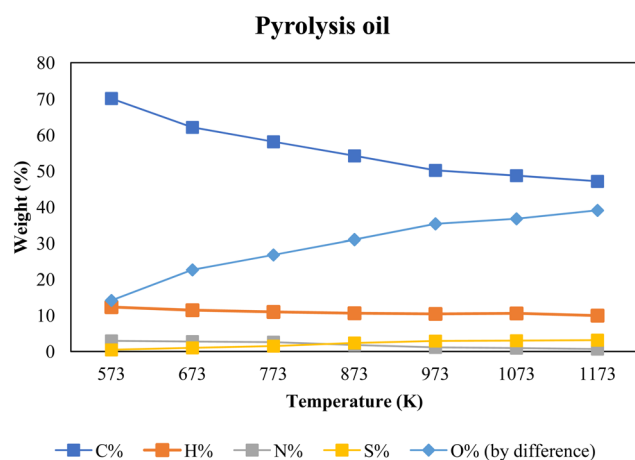
Fig. 11 Effect of CHNSO composition on pyrolysis oil.

gaseous products. These fractured gaseous components tend to retain carbon, thereby reducing the carbon content in the remaining pyrolysis oil. At higher temperatures, thermal

cracking becomes more pronounced, leading to the production of carbon-rich, lower molecular weight gases. Table 7 summarizes the identified compounds in the pyrolysis oil obtained at 873 K, including their retention times and potential applications. The GC-MS analysis indicates that many of the detected components incorporate oxygen within their molecular structures, which is consistent with the elevated oxygen content observed.

The underlying mechanisms responsible for the variations in oxygen and carbon content with increasing temperature may be further elucidated through a detailed stoichiometric analysis of the primary and secondary pyrolysis reactions. The pyrolysis oil obtained at 873 K exhibited a dark brown color and smoky appearance. Several new compounds were identified, including D-limonene, various decanes, phenol, benzene, and phenyl derivatives. These constituents exhibit both aromatic and aliphatic characteristics. Due to their broad range of potential applications, the presence of such compounds enhances the value proposition of converting orange peel waste into pyrolytic oil.

Table 7 Summary of the identified compounds (based on GC–MS analysis) in pyrolysis oil obtained at 873 K, including their retention times and potential applications

Peaks	Retention time (min)	Area of the component under the curve %	Compound name	Molecular weight	Applications
1	2.13	11.89	1,2-Dimethyl benzene (C_8H_{10})	106	Printing, leather, and rubber industries[112]
2	2.81	8.25	2,3 Butanedione ($C_4H_6O_2$)	86	Production from glucose by fermentation[113]
3	3.35	9.52	D-limonene ($C_{10}H_{16}$)	136	Cosmetic usage[114]
4	4.55	1.89	Acetophenone ($C_9H_{10}O_3$)	166	Used for the manufacture of soaps, detergents, lotions, creams, and perfumes[115]
5	6.66	1.46	(4E,6Z)-2,6-dimethyl-2,4,6 octatriene ($C_{10}H_{16}$)	136	Used as a perfume component[113]
6	7.44	2.45	Acetic acid ($C_2H_4O_3$)	76	For pharmaceutical application[58,116]
7	7.85	0.86	1,2,3 Trimethyl benzene (C_9H_{12}	120	It is derived from the C9 aromatic fraction in petroleum distillation or synthesized via toluene and xylene methylation[113]
8	10.41	2.62	1,4 -Diethyl benzene ($C_{10}H_{14}$)	134	In nanotechnology[117]
9	10.62	8.89	Citronellal ($C_{10}H_{18}O$)	154	Used as a robust antifungal qualifier[118]
10	10.75	6.11	Octantal ($CH_3(CH_2)6CHO$)	128	For the perfume and food industries[119]
11	11.40	0.86	Phenol (C_6H_6O)	94	Used medically to help sore throat[119]
12	11.53	1.44	Glycerin ($C_3H_8O_3$)	92	Used in the cosmetic industry[120]
13	12.51	1.56	Methyl hydroquinone ($C_6H_6O_2$)	110	For skin whitening[121]
14	13.78	9.05	Guaiacol ($C_7H_8O_2$)	124	Precursor to various flavorants[122]
15	14.62	9.96	4-Propyl guaiacol ($C_{10}H_{14}O_2$)	166	Medicinal use as an antiseptic and a local anesthetic[122]
16	17.86	2.23	Acetosyringone ($C_{10}H_{12}O_4$)	196	Allows higher transformation efficiency in plants[123]
17	18.76	2.01	Levoglucosan ($C_6H_{10}O_5$)	162	Synthesis of chiral polymers such as nonhydrolyzable glucose polymers[124]
18	19.08	4.45	2,4 Xylenol ($C_8H_{10}O$)	122	Antioxidant[113]
19	20.35	1.08	Hexanal, 4-methyl ($C_7H_{14}O$)	114	Used as a flavoring agent[125]
20	22.86	2.85	4-Ethyl-catechol ($C_8H_{10}O_2$)	138	Perfume and pharma industries[113]
21	24.57	2.45	Heptadecanenitrile ($C_{17}H_{33}N$)	251	Used as a solvent and in polycarboxylic acid production[34]
22	25.99	1.76	Oleic acid ($C_{18}H_{34}O_2$)	282	Used for the food and cosmetic industry[126]
23	26.40	1.03	Stearic acid ($C_{18}H_{36}O_2$)	284	Used for the food and cosmetic industry[126]
24	28.60	1.17	Arachic acid ($C_{20}H_{40}O_2$)	312	Used in the pharmaceutical industry[127]
25	30.35	0.98	Monoplamitin ($C_{19}H_{38}O_4$)	330	Used in drug delivery systems[128]
26	32.65	0.83	Squalene ($C_{30}H_{50}$)	410	Used for the cosmetic industry[129]
27	33.40	0.66	n-Tetracosane ($C_{24}H_{50}$)	338	Used as a solvent and also in microencapsulation[130]
28	37.98	0.14	β-Silosterol ($C_{29}H_{50}O$)	414	Lowering cholesterol levels and improving symptoms of an enlarged prostate (BPH)[131]
29		1.55	Unidentified		
30		$\sum = 100$			

Table 8 GC analysis of pyrolysis gas derived from orange peel waste

Feedstock	N_2	CO_2	CO	CH_4	H_2	C_2H_2	C_2H_6	C_3H_8	NO_x	CO/H_2
Orange peel waste	55.4	2.00	2.89	10.28	7.43	9	6	5	2	1/2.57

3.6.3 GC-MS analysis of the pyrolysis oil. The pyrolysis oil derived from orange peel waste was subjected to both quantitative and qualitative characterization. GC-MS analysis was performed using an Agilent 6890 system equipped with an HP-5 column (0.25 μm × 30 m × 0.25 mm) and a 5973 mass selective detector (MSD).[111] The analysis identified several novel compounds, comprising a mixture of aromatic and aliphatic constituents. Notable compounds included D-limonene, furfural, propanol, benzene, phenyl derivatives, and cyclopentane-1-hydroxymethyl-1,3-dimethyl. These findings are

in agreement with the work of Abidi *et al.*,[79] who identified similar components such as D-limonene, acetophenone, acetic acid, glycerin, hydroquinone, levoglucosan, hexanal (4-methyl), oleic acid, and stearic acid. The presence of these compounds, many of which possess industrial relevance, underscores the potential of pyrolysis oil as a source of value-added chemicals, further highlighting the appeal of the pyrolysis process for biomass valorization.

3.6.4 GC analysis of pyrolysis gas.

GC analysis of pyrolysis gas derived from orange peel waste is summarized in Table 8. The primary constituents of the pyrolysis gas include CO, CO_2, H_2, CH_4, C_2H_2, C_2H_6, C_3H_8, and NO_x. At 873 K, the gas exhibited a CO/H_2 ratio of 1 : 2.57, an HHV of 19.87 MJ m^{-3}, and a LHV of 18.38 MJ m^{-3}. These results align with previous studies.[14] Comparison with data reported in ref. 85, in which pyrolysis was conducted at temperatures ranging from 573 K to 773 K, shows that the yields of CO, CO_2, CH_4, H_2, and N_2 varied between 10.78–59.79%, 0.12–0.68%, 0.42–3.57%, 0.46–0%, and 88.09–34.33%, respectively. The current study, performed at 873 K, observed substantial quantities of these gases, consistent with increased gas yield and composition shifts at elevated temperatures.

4. Cost estimation

4.1. Evaluation of process capital expenditures

This study evaluates the revenue potential of products derived from the pyrolysis of orange peel waste by scaling up the pilot-scale capacity to 10 kg per batch. The projected total capital expenditure for this process, which yields pyrolysis char, oil, and gas, is estimated at $19258.69 ($1 = ₹85.39, dated 24.05.2025). This estimate encompasses the total project cost (TPC), total plant direct cost (TPDC), total plant indirect cost (TPIC), contractor's profit and charges (CPC), 5% working capital, and an initial expense equal to 10% of the debt financing cost (DFC). A detailed breakdown of the required initial investment for the pyrolysis of waste orange peels is provided in Table S2 (SI).[61] The majority of capital costs $69331.30 are attributed to machinery setup, system installation, electrical controls, site upgrades, piping, and ancillary infrastructure. Rajendran *et al.*[41] reported that the process

equipment cost (PEC) contributed 20.9% to the total cost of bio-oil production from pine sawdust using microwave pyrolysis; similarly, in the present study, PEC accounts for 17.4% of the total cost. The equipment investment for the pyrolysis process with a 10 kg h^{-1} capacity is $ 19 258.69, which is higher than that reported by Fajimi and Oboirien[132] (*i.e.*, $594.312), whose study covered capacities of 30 tons per day, 60 tons per day, and 120 tons per day for fluidized, fixed, and rotary kiln bed systems, respectively. The process investment cost of the present study is comparable to that reported by Alawa *et al.*,[133] for a reactor with 10 kg h^{-1} capacity. Variations in investment cost arise from country-specific factors such as tax structures, inflation and interest rates, energy tariffs, and differences in process parameters.

In summary, this investigation presents the first economic analysis of the pyrolysis process applied to orange peel waste. Equipment procurement accounted for 17.4% of the total capital expenditure, while 45.2% was allocated to installation components, including pipelines, instrumentation and control systems, electrical setups, buildings, yard improvements, and service facilities. The most significant expenses were related to reactor fabrication, the pyrolysis chamber, the cooler condenser, and the nitrogen cylinder. The initial capital investment required for the pyrolysis of orange peel waste is shown in Fig. 12. The TPIC summarises 44.5% of engineering and 55.4% of building-related expenses. TPIC represents 12.9% of the capital cost, while the CFC accounts for 11.5%.

4.2. Evaluation of process operational expenses

The detailed breakdown of the operational investment cost for the pyrolysis of orange peel waste is presented in Table S3 (SI). The operational expenses associated with the pyrolysis of orange peel waste are presented in Fig. 13. Total operational expenses amounted to $10,163.08. Variable costs ($10,203.08) were substantially lower than fixed costs ($96,293.48). Among the variable expenses, utilities contributed the largest share at 58.1%, followed by raw materials (9.2%), consumables (7.9%), transportation (3.5%), and other miscellaneous costs (20.9%). The economic analysis was performed for feedstock input rates of 2 kg h^{-1}, 4 kg h^{-1}, and 10 kg h^{-1}, with 10 kg h^{-1} selected to ensure scalability and commercial feasibility.
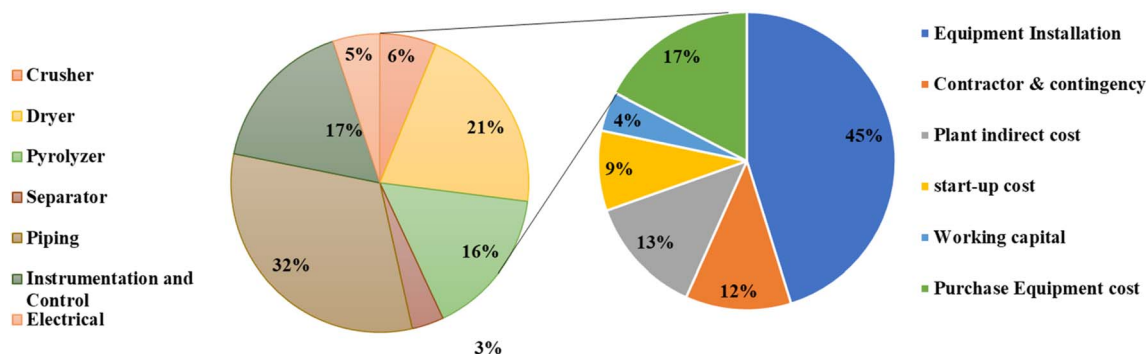

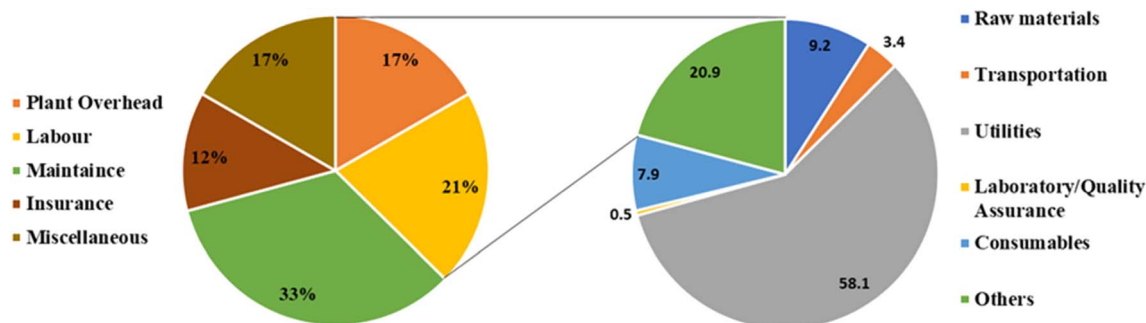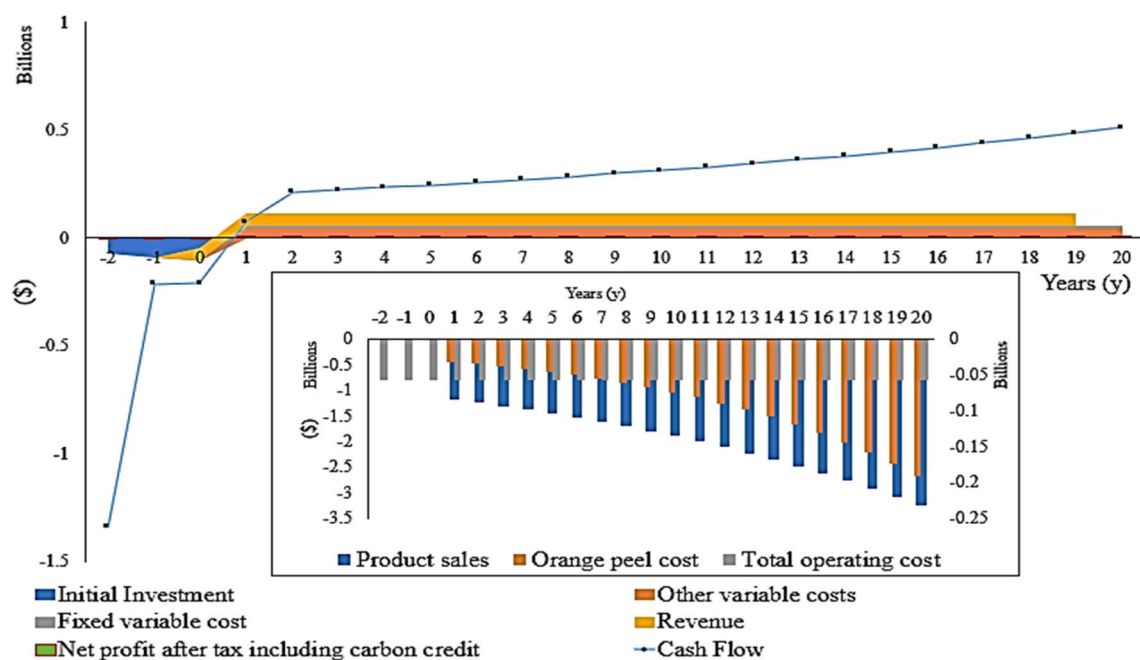**Fig. 12** Initial capital investment required for the pyrolysis of orange peel waste.
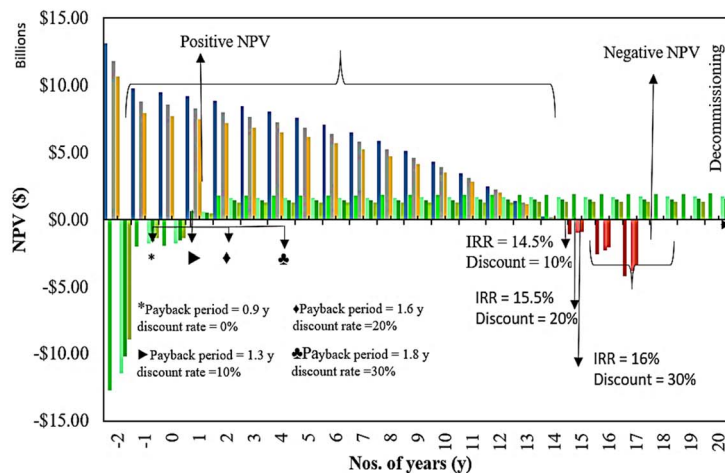
Fig. 13 Operational expenses associated with the pyrolysis of orange peel waste.

(a)

(b)

Fig. 14 Orange pyrolysis plant, (a) expenditures and income, and (b) financial statistics for the life period.

The total operational expenditure of $20366.15 is significantly lower than those reported by Selvam *et al.*[134] (*i.e.*, $ 246 044.10) from other biomass feedstocks. This investigation primarily focuses on the primary pyrolysis of orange peel waste, with a cost estimation of $117478.04. The economic analysis is based on product generation at a laboratory scale and is intended to provide a foundational framework for scaling up the process. Due to the lack of reliable market data for pyrolysis char derived from orange peel waste, its selling price was estimated at ₹9.5 kg^{-1} ($\approx$\$0.11), based on comparable listings from previous researchers[37] (http://www.indiamart.com). The market values of pyrolysis oil and gas were considered at ₹95 kg^{-1} ($\approx$\$1.11) and ₹44 kg^{-1} ($\approx$\$0.52), respectively. The price of pyrolysis oil was adopted from the commercial biodiesel rate reported by Alawa *et al.*,[133] while the gas price was assumed as a reasonable intermediate value due to the absence of specific market data. All product prices were based on prevailing market conditions in India.

4.3. Analyzing the profitability of pyrolyzing orange peel waste

Economists utilize the NPV metric to assess the profitability of the project. A positive NPV indicates financial viability and a high return on investment (ROI), making the project an attractive investment opportunity.[135] The corresponding cash flow sheet is provided in Table S4 (SI). Assuming an annual yield of 331 776 kg of pyro-char, pyro-oil, and pyro-gas over a 20-year operational period, with daily operations of 8 h, the projected revenue amounts to $20366.15, which is the breakeven point. Pyrolysis products have diverse applications: pyro-char can be used as a fertilizer, a soil conditioner, or as an electrode material in wastewater treatment; pyro-oil is suitable for transportation due to its physicochemical similarity to conventional diesel and petrol; and pyro-gas, composed primarily of CO, CO_2, CH_4, and H_2, can serve as an eco-fuel or as a hydrogen source for sustainable energy and electricity generation.[136] Therefore, price
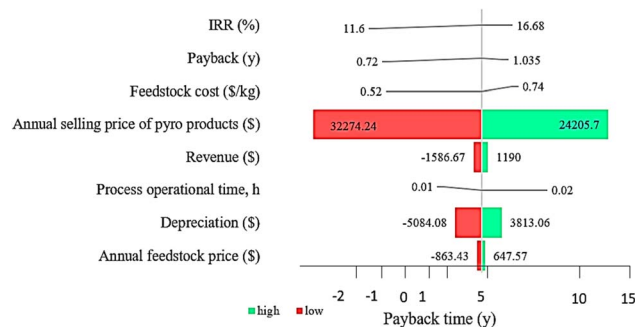

Fig. 16 Tornado plot illustrating the relative impact of modifying specific processes and economic factors on orange peel waste pyrolysis.

also can vary based on the applications. The present investigation estimates a net payback period of 0.9 years at an interest rate of 7.5% and equity contribution of 40%, consistent with findings by Selvam *et al.*[134] and Chhabra *et al.*[68] As discount rates of 10%, 20%, and 30% are applied, the payback period increases from 1.3 years to 1.8 years and IRR also changes from 14.5% to 16%. Prior studies have reported varying financial indicators: for instance, a study on rotary kiln plant[66] achieved an ROI of 32.6%, an IRR of 29%, and a payback period of 6.2 years; a facility processing 50 000 t year^{-1} reported a 3.6-year payback, which decreased to 1.59 years for a 500 000 t year^{-1} plant. Initially, the NPV is negative at a 10% discount rate but becomes positive when the IRR reaches 33.3%, assuming a 20-year operational timeframe before decommissioning. Further financial details are illustrated in Fig. 14a (expenditure and income) and 14b (financial statistics for the life period).

This study emphasizes mass production, with the plant scale-up from 10 kg h^{-1} to 10 000 kg h^{-1}. The projected annual profit from orange peel waste pyrolysis at varying plant capacities is illustrated in Fig. 15. Application of the power law model (see eqn (14)) indicates that increasing plant capacity leads to
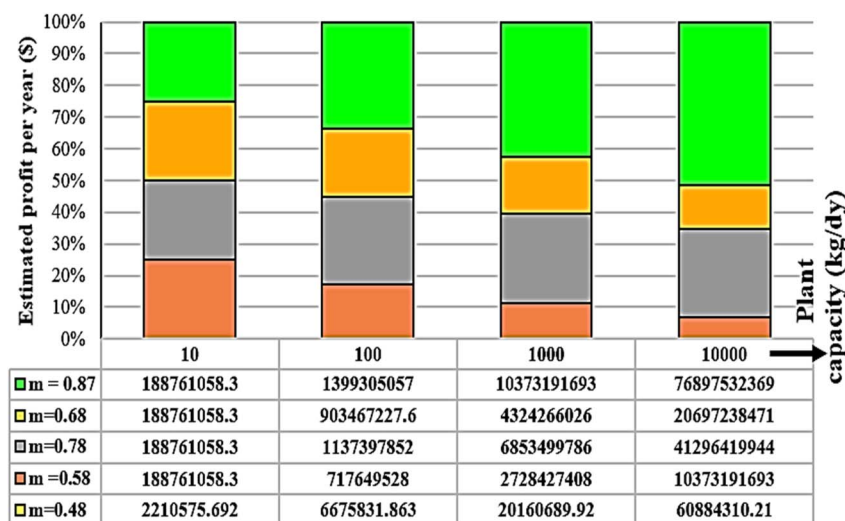

Fig. 15 Projected annual profit from orange peel waste pyrolysis at varying plant capacities.

a substantial rise in annual profits. The current investigation also demonstrates a shortened payback period of approximately 2 years, highlighting the process's strong economic feasibility. Whether operated at the current capacity or through future scale-up, the process proves more advantageous than previously reported methods.

4.4. Sensitivity analysis

A sensitivity analysis was conducted to evaluate the influence of key parameters on the project's economic viability. Fig. 16 illustrates the relative influence of process modifications and economic factors on the pyrolysis of orange peel waste. The baseline scenario assumed a feedstock cost of $2968.03 annually, daily operation of 8 h, and product selling prices of $0.11 kg^{-1} for pyro-char, $1.11 L^{-1} for pyro-oil, and $0.52 L^{-1} for pyro-gas, resulting in a payback period of 1.3 years and an IRR of 14.5%. Increasing the feedstock cost to $0.70 kg^{-1} extended the payback period to 1.04 years and slightly increased the IRR to 16.68%. Conversely, reducing the feedstock cost to $0.52 kg^{-1} shortened the payback period to 0.72 years, while slightly decreasing the IRR to 11.6%, consistent with the findings of Varshney *et al.*[137] Among the assessed economic factors, the IRR, plant scale, and waste disposal charges exhibited more pronounced effects on the minimum selling price (MSP) than feedstock cost. For example, waste disposal charges of ₹4326 ton^{-1} (*i.e.*, $50 ton^{-1}) and ₹8653 ton^{-1} (*i.e.*, $100 ton^{-1}) reduced the MSP by 16.2% and 32.5%, respectively. The analysis highlights that optimizing the plant scale and minimizing waste disposal charges are critical to enhancing economic feasibility, as variations in key parameters such as raw material costs and operational expenses significantly influence both the NPV and MSP.

5. Conclusion

This study presents a sustainable approach to managing waste orange peels through pyrolysis, yielding three valuable products: pyro-char, pyro-oil, and pyro-gas. Pyro-char demonstrates significant potential for industrial applications, particularly in the adsorption of hazardous substances in effluent and gas treatment processes, while pyro-oil and pyro-gas emerge as promising alternatives to fossil fuels. The study identified feedstock mass, reaction temperature, and heating rate as critical parameters influencing pyrolysis performance. Optimal conditions—comprising a feedstock mass of 2 kg, a temperature of 873 K, and a heating rate of 20 K min^{-1}—resulted in maximum yields of 26.52 wt% for pyro-char, 22.76 wt% for pyro-oil, and 50.72 wt% for pyro-gas, with an overall process desirability of 0.7. The experimental results produced a pyro-char yield of 28.12%, pyro-oil yield of 22.89%, and pyro-gas yield of 48.99%, aligning with theoretical predictions within ±5.7% margin. The estimated payback period for the initial investment is 1.3 years, substantially shorter than the 6 years typically reported for pyrolysis gas and pyrolysis oil production. The IRR is estimated at 16%, with both positive and negative NPV scenarios considered, highlighting the process's financial

sensitivity. A sensitivity analysis further affirmed the economic viability of the system. The products exhibit high volatile content, predominantly composed of hydroxyl and ether functional groups, suggesting potential for automotive fuel applications. This work underscores a sustainable pathway for converting biomass waste into value-added products, aligning with Industry 5.0 principles and advancing the United Nations 2030 sustainability goals for environmental and societal impact.

Conflicts of interest

There are no conflicts of interest to disclose.

Data availability

The data that supports the findings of this study are available in the supplementary information (SI) material of this article. Supplementary information is available. See DOI: https://doi.org/10.1039/d5su00575b.

Acknowledgements

References

1 D. V. Suriapparao, R. Vinu, A. Shukla and S. Haldar, *Bioresour. Technol.*, 2020, **302**, 122775.

2 S. Shafiee and E. Topal, *Energy Policy*, 2009, **37**, 181–189.

3 U. S. Behera and J. S. Sangwai, *Ind. Eng. Chem.*, 2021, **60**, 291–313.

4 U. Michael-Igolima, S. J. Abbey, A. O. Ifelebuegu and E. U. Eyo, *Materials*, 2023, **16**, 1092.

5 F. Chivrac, E. Pollet and L. Avérous, *Mater. Sci. Eng. R Rep.*, 2009, **67**, 1–17.

6 J. S. Yaradoddi, N. R. Banapurmath, S. V. Ganachari, M. E. M. Soudagar, A. M. Sajjan, S. Kamat, M. A. Mujtaba, A. S. Shettar, A. E. Anqi, M. R. Safaei, A. Elfasakhany, M. I. H. Siddiqui and M. A. Ali, *J. Mater. Res. Technol.*, 2022, **17**, 3186–3197.

7 D. Neves, H. Thunman, A. Matos, L. Tarelho and A. Gómez-Barea, *Prog. Energy Combust. Sci.*, 2011, **37**, 611–630.

8 A. Selvarajoo, Y. L. Wong, K. S. Khoo, W. H. Chen and P. L. Show, *Chemosphere*, 2022, **294**, 1333671.

9 R. Miranda, D. Bustos-Martinez, C. S. Blanco, M. H. G. Villarreal and M. E. R. Cantú, *J. Anal. Appl. Pyrolysis*, 2009, **86**, 245–251.

10 K. Sahoo, A. Kumar and J. P. Chakraborty, *J. Mater. Cycles Waste Manag.*, 2021, **23**, 186–204.

11 K. Chaiwong, T. Kiatsiriroat, N. Vorayos and C. Thararax, *Biomass Bioenergy*, 2013, **56**, 600–606.

12 A. Amrullah, O. Farobie and G. P. Pramono, *Korean J. Chem. Eng.*, 2022, **39**, 389–397.

13 A. Amrullah, O. Farobie, H. Irawansyah, M. Lutfi and L. N. Haty, *Process Saf. Environ. Prot.*, 2024, **187**, 471–482.

14 S. Poddar, J. N. Ullas Krishnan and J. S. Chandra Babu, *Indian Chem. Eng.*, 2022, **64**, 433–460.

15 K. Yamini, K. Sandeep Charan, S. Poddar and J. S. C. Babu, *Biomass Convers. Biorefin.*, 2023, **13**, 15903–15916.

16 M. J. Antal, S. G. Allen, X. Dai, B. Shimizu, M. S. Tam and M. Grønli, *Ind. Eng. Chem. Res.*, 2000, **39**, 4024–4031.

17 M. Tripathi, J. N. Sahu and P. Ganesan, *Renew. Sustain. Energy Rev.*, 2016, **55**, 467–481.

18 L. Tripathi, A. K. Mishra, A. K. Dubey, C. B. Tripathi and P. Baredar, *Renewable Sustainable Energy Rev.*, 2016, **60**, 226–233.

19 O. Soka and O. Oyekola, *Heliyon*, 2020, **6**, e043446.

20 R. Xiao and W. Yang, *Renewable Energy*, 2013, **50**, 136–141.

21 P. T. Williams and S. Besler, *Renewable Energy*, 1996, **7**, 233–250.

22 G. Lezcano, R. Gautam, I. Hita, A. Yerrayya, J. Aljaziri, B. B. de Feitas, V. Samaras, K. J. Lauersen, S. M. Sarathy and P. Castano, *J. Anal. Appl. Pyrolysis*, 2025, **191**, 107170.

23 Z. Xiong, Y. Wang, S. S. A. Syed-Hassan, X. Hu, H. Han, S. Su, K. Xu, L. Jiang, J. Guo, E. E. S. Berthold, S. Hu and J. Xiang, *Energy Convers. Manag.*, 2018, **163**, 420–427.

24 H. S. Choi, Y. S. Choi and H. C. Park, *Korean J. Chem. Eng.*, 2010, **27**, 1164–1169.

25 M. Pahnila, A. Koskela, P. Sulasalmi and T. Fabritius, *Energies*, 2023, **16**, 6939.

26 A. Hornung, *Transformation of Biomass: Theory to Practice*, Wiley Online Library, 2014.

27 N. Bucher, *Angew. Chem.*, 1981, **93**, 625.

28 A. O. Oyedun, K. L. Lam, T. Gebreegziabher and C. W. Hui, *Appl. Therm. Eng.*, 2013, **61**, 123–127.

29 C. Y. Yang, X. M. Yang, X. S. Lu, J. Z. Yao and W. G. Lin, *Chin. J. Process Eng.*, 2005, **5**, 379–383.

30 M. Afraz, F. Muhammad, J. Nisar, A. Shah, S. Munir, G. Ali and A. Ahmad, *Waste Manag. Bull.*, 2024, **1**, 30–40.

31 R. Naveenkumar and G. Baskar, *Bioresour. Technol.*, 2021, **320**, 124347.

32 O. A. Fakayode and K. E. Abobi, *J. Anal. Sci. Technol.*, 2018, **9**, 20.

33 A. K. Tovar, L. A. Godínez, F. Espejel, R. M. Ramírez-Zamora and I. Robles, *Waste Manag.*, 2019, **85**, 202–213.

34 A. Sharma, M. Noda, M. Sugiyama, A. Ahmad and B. Kaur, *Molecules*, 2021, **26**, 4671.

35 I. Kariim, Y. O. Waidi, H. Swai and T. Kivevele, *J. Anal. Appl. Pyrolysis*, 2023, **173**, 106032.

36 N. K. Sharma, R. Savithri, A. Kamal, A. Kaur, P. Ram and R. K. Rao, *ENERGY STATISTICS India 2021*, Delhi, 2021.

37 U. S. Behera, S. Poddar and H.-S. Byun, *Sustain. Energy Fuels*, 2025, 1–22.

38 Z. Yao, D. C. Makepa, S. Poddar, M. Reinmoller, M. Bertelsen, J. Jiang, J. Tong, J. Cui, J. Liu and I. M. D. C. Cordeiro, *Case Stud. Therm. Eng.*, 2025, **71**, 106228.

39 H. Park, J. Byun and J. Han, *Energy*, 2021, **230**, 120729.

40 C. D. Scown, N. R. Baral, M. Yang, N. Vora and T. Huntington, *Curr. Opin. Biotechnol.*, 2021, **67**, 58–64.

41 N. Rajendran, D. Kang, J. Han and B. Gurunathan, *J. Clean. Prod.*, 2022, **365**, 132712.

42 M. Ortiz-Sanchez, J. C. Solarte-Toro, C. E. Orrego-Alzate, C. D. Acosta-Medina and C. A. Cardona-Alzate, *Biomass Convers. Biorefin.*, 2021, **11**, 645–659.

43 M. Ortiz-Sanchez, J. C. Solarte-Toro, P. J. Inocencio-García and C. A. Cardona Alzate, *Enzyme Microb. Technol.*, 2024, **172**, 110327.

44 M. Ortiz-Sanchez, C. A. C. Alzate and J. C. Solarte-Toro, *Biomass*, 2024, **4**, 107–131.

45 M. Ladaniya, *Citrus Fruit: Biology, Technology and Evaluation, Second Edition*, Academic Press, 2022.

46 M. Ladanyia and M. Ladaniya, *Citrus Fruit: Biology, Technology and Evaluation*, Academic Press, 2010.

47 N. Bhattacharjee and A. B. Biswas, *J. Environ. Chem. Eng.*, 2019, **7**, 10290301–10290316.

48 E. Shayan, V. Zare and I. Mirzaee, *Energy Convers. Manag.*, 2018, **159**, 30–41.

49 L. A. Hamilton and J. F. Kennedy, *Sourcebook of Methods of Analysis for Biomass and Biomass Conversion Processes*, Springer Netherlands, Netherlands, 1992.

50 A. Oasmaa, E. Leppämäki, P. Koponen, J. Levander and E. Tapola, *Physical Characterisation of Biomass-Based Pyrolysis Liquids Application of Standard Fuel Oil Analyses*, VTT Technical Research Centre of Finland, Espoo, 1st edn, 1997.

51 T. Waldheim and L. Nilsson, *Heating Value of Gases from Biomass Gasification*, Nyköping, 2001.

52 R. Myres, D. Montgomery and C. Anderson, *Process and Product Optimization Using Designed Experiments*, Wiley, New York, 4th edn, 2009, vol. 4.

53 L. Vera Candioti, M. M. De Zan, M. S. Cámara and H. C. Goicoechea, *Talanta*, 2014, **124**, 123–138.

54 U. S. Behera, P. C. Mishra and G. B. Radhika, *Water Sci. Technol.*, 2022, **85**, 515–534.

55 S. B. Imandi, V. V. R. Bandaru, S. R. Somalanka, S. R. Bandaru and H. R. Garapati, *Bioresour. Technol.*, 2008, **99**, 4445–4450.

56 J. Zolgharnein, M. Bagtash and N. Asanjarani, *J. Environ. Chem. Eng.*, 2014, **2**, 988–1000.

57 R. F. Schmid, R. M. Bernard, E. Borokhovski, R. M. Tamim, P. C. Abrami, M. A. Surkes, C. A. Wade and J. Woods, *Comput. Educ.*, 2014, **72**, 271–291.

58 S. Halder, U. S. Behera, S. Poddar, J. Khanam and S. Karmakar, *AAPS PharmSciTech*, 2024, **25**, 16201–16221.

59 K. Sahoo, U. S. Behera, S. Poddar and H.-S. Byun, *Korean J. Chem. Eng.*, 2024, **41**, 2621–2638.

60 A. El-Ghenymy, S. Garcia-Segura, R. M. Rodríguez, E. Brillas, M. S. El Begrani and B. A. Abdelouahid, *J. Hazard. Mater.*, 2012, **221–222**, 288–297.

61 T. Sfetsas, C. Michailof, A. Lappas, Q. Li and B. Kneale, *J. Chromatogr. A*, 2011, **1218**, 3317–3325.

62 H. N. Jeong, R. H. Kwon, Y. Kim, S. H. Yoo, S. M. Yoo and C. Do Wee, *Foods*, 2023, **12**, 1104.

63 M. Peters, K. Timmerhaus and R. West, *Equipment Costs Plant Design and Economics for Chemical Engineers*, 5th edn, 2004.

64 F. P. Goksal, *Heliyon*, 2022, **8**, e11669.

65 R. Bi, Y. Zhang, X. Jiang, H. Yang, K. Yan, M. Han, W. Li, H. Zhong, X. Tan, L. Xia, X. Sun and S. Xiang, *Energy*, 2022, **260**, 125039.

66 S. Jenkins, *Chemical Engineering Plant Cost Index Annual Average - Chemical Engineering*, 2019, p. 1, https://www.chemengonline.com/2019-chemical-engineering-plant-cost-index-annual-average/, accessed 11 November 2024.

67 W. D. Seider, R. Gani, S. Widagdo, K. M. Ng, J. D. Seider and D. R. Lewin, *Product and Process Design Principles: Synthesis, Analysis and Evaluation*, Wiley, New York, 4th edn, 2016.

68 V. Chhabra, A. Parashar, Y. Shastri and S. Bhattacharya, *Ind. Eng. Chem. Res.*, 2021, **60**, 1473–1482.

69 K. Kishor, *Koshi Motors & Fabrication Private Limited*, https://www.indiamart.com/koshi-motors-fabrication/profile.html, accessed 11 November 2024.

70 J. B. Shah and J. B. Valaki, *J. Kejuruteraan*, 2022, **34**, 495–504.

71 A. E. M. Fodah, M. K. Ghosal and D. Behera, *Int. J. Energy Res.*, 2021, **45**, 5679–5694.

72 L. K. S. Gujjala and W. Won, *Bioresour. Technol.*, 2022, **364**, 128028.

73 A. Arora, J. Banerjee, R. Vijayaraghavan, D. MacFarlane and A. F. Patti, *Ind. Crops Prod.*, 2018, **116**, 24–34.

74 J.-H. Kim, T. Lee, Y. F. Tsang, D. H. Moon, J. Lee and E. E. Kwon, *Sci. Total Environ.*, 2024, **941**, 173701.

75 A. T. Koçer, D. Özçimen and İ. Gökalp, *Biomass Convers. Biorefin.*, 2024, **14**, 22839–22851.

76 K. Açıkalın, *Biomass Convers. Biorefin.*, 2022, **12**, 501–514.

77 Y. Zhu, G. Xu, W. Song, Y. Zhao, Z. Miao, R. Yao and J. Gao, *J. Energy Inst.*, 2021, **98**, 172–178.

78 M. A. Lopez-Velazquez, V. Santes, J. Balmaseda and E. Torres-Garcia, *J. Anal. Appl. Pyrolysis*, 2013, **99**, 170–177.

79 S. Abidi, A. B. H. Trabelsi and N. Boudhrioua, *J. Mater. Cycles Waste Manag.*, 2023, **25**, 235–248.

80 F. Ateş, E. Pütün and A. E. Pütün, *J. Anal. Appl. Pyrolysis*, 2004, **71**, 779–790.

81 B. Zapata, J. Balmaseda, E. Fregoso-Israel and E. Torres-García, *J. Therm. Anal. Calorim.*, 2009, **98**, 309–315.

82 X. Wang, Z. Hu, S. Deng, Y. Wang and H. Tan, *Environ. Prog. Sustain. Energy*, 2015, **34**, 923–932.

83 D. Mohan, C. U. Pittman and P. H. Steele, *Energy Fuels*, 2006, **20**, 848–889.

84 A. K. Varma and P. Mondal, *J. Therm. Anal. Calorim.*, 2016, **124**, 487–497.

85 G. Bensidhom, A. Ben Hassen-Trabelsi, K. Alper, M. Sghairoun, K. Zaafouri and I. Trabelsi, *Bioresour. Technol.*, 2018, **247**, 363–369.

86 V. Dhyani and T. Bhaskar, *Renewable Energy*, 2018, **129**, 695–716.

87 A. Aboulkas, H. Hammani, M. El Achaby, E. Bilal, A. Barakat and K. El harfi, *Bioresour. Technol.*, 2017, **243**, 400–408.

88 M. Boluda-Aguilar and A. López-Gómez, *Ind. Crops Prod.*, 2013, **41**, 188–197.

89 M. Ghodrat, J. A. Alonso, D. Hagare, R. Yang and B. Samali, *Int. J. Environ. Sci. Technol.*, 2019, **16**, 3721–3734.

90 M. Ghodrat, M. A. Rhamdhani, G. Brooks, S. Masood and G. Corder, *J. Clean. Prod.*, 2016, **126**, 178–190.

91 M. T. H. Siddiqui, S. Nizamuddin, N. M. Mubarak, K. Shirin, M. Aijaz, M. Hussain and H. A. Baloch, *Waste Biomass Valorization*, 2019, **10**, 521–532.

92 K. Intani, S. Latif, A. K. M. R. Kabir and J. Müller, *Bioresour. Technol.*, 2016, **218**, 541–551.

93 O. T. Ore and F. M. Abebiyi, *Unconv. Resour.*, 2024, **4**, 100080.

94 N. M. Mubarak, F. Yusof and M. F. Alkhatib, *Chem. Eng. J.*, 2011, **168**, 461–469.

95 A. M. Nusrat Aman, A. Selvarajoo, T. L. Lau and W. H. Chen, *Chemosphere*, 2023, **313**, 137477.

96 S. Gupta and H. W. Kua, *Sci. Total Environ.*, 2019, **662**, 952–962.

97 K. Yadav and S. Jagadevan, *Bioenergy Res.*, 2021, **14**, 964–977.

98 U. S. Behera, S. Poddar and H.-S. S. Byun, *J. Chem. Technol. Biotechnol.*, 2024, **99**, 1212–1224.

99 D. C. Montgomery, *Design and Analysis of Experiments, 10th Edition, Wiley*, Wiley Online Library, 10th edn, 2020.

100 D. C. Montgomery, *Design and Analysis of Experiments*, Wiley, New York, 10th edn., 2019.

101 L. E. Hernandez-Mena., A. A. B. Pecora and A. L. Beraldo, *Chem. Eng. Trans.*, 2014, **37**, 115–120.

102 C. M. Santos, J. Dweck, R. S. Viotto, A. H. Rosa and L. C. de Morais, *Bioresour. Technol.*, 2015, **196**, 469–479.

103 S. S. Lam, R. K. Liew, X. Y. Lim, F. N. Ani and A. Jusoh, *Int. Biodeterior. Biodegrad.*, 2016, **113**, 325–333.

104 A. Y. Elnour, A. A. Alghyamah, H. M. Shaikh, A. M. Poulose, S. M. Al-Zahrani, A. Anis and M. I. Al-Wabel, *Appl. Sci.*, 2019, **9**, 1149.

105 N. Ayrilmis, J. H. Kwon, T. H. Han and A. Durmus, *Mater. Res.*, 2015, **18**, 654–659.

106 O. Das, D. Bhattacharyya and A. K. Sarmah, *J. Clean. Prod.*, 2016, **129**, 159–168.

107 Z. Chen, B. Lin, Y. Huang, Y. Liu, Y. Wu, R. Qu and C. Tang, *Sci. Total Environ.*, 2023, **862**, 160860.

108 S. Kordoghli, E. Fassatoui, J. F. Largeau and B. Khiari, *C. R. Chim.*, 2023, **26**, 37–51.

109 H. M. Yang, S. Appari, S. Kudo, J. I. Hayashi and K. Noringa, *Ind. Eng. Chem. Res.*, 2015, **54**, 6855–6864.

110 J. W. C. Tae-Seung Kim, S. Oh, J.-Y. Kim and In-G. Choi, *Energy*, 2014, **68**, 437–443.

111 J. Mathias, *A Beginner's Guide: How to Interpret Gas Chromatography Mass Spectrometry Results*, https://www.innovatechlabs.com/newsroom/1841/how-to-interpret-gas-chromatography-mass-spectrometry-results/#:~:text=TypicallyCthey-axisC,atthepointofretention, accessed 4 October 2024.

112 B. Blu-tack, *Identification of the Substance/preparation and of the Company/undertaking*, SWEDEN, 2016.

113 S. S. Chadwick, *Ullmann's Encyclopedia of Industrial Chemistry*, 2000.

114 Healthline, *What Is Limonene? Everything You Need to Know*, https://www.healthline.com/nutrition/grapefruit-essential-oil#TOC_TITLE_HDR_9, accessed 24 September 2024.

115 N. Berova, G. A. Ellestad and N. Harada, *Reference Module in Chemistry, Molecular Sciences and Chemical Engineering*, 2010, 9, pp. 91–146.

116 S. Karmakar, S. Poddar and J. Khanam, *AAPS PharmSciTech*, 2022, **23**, 25601–25623.

117 R. Pawlak, L. Nony, F. Bocquet, V. Oison, M. Sassi, J. M. Debierre, C. Loppacher and L. Porte, *J. Phys. Chem. C*, 2010, **114**, 9290–9295.

118 P. S. Auerbach, H. J. Donner and E. A. Weiss, in *Field Guide to Wilderness Medicine*, ed. P. S. Auerbach, H. J. Donner and E. A. Weiss, Mosby. Inc, 3rd edn, 2008, pp. 453–473.

119 H. Jung, E. H. Lee, T. H. Lee and M. H. Cho, *Int. J. Mol. Sci.*, 2016, **17**, 1449.

120 L. C. Becker, W. F. Bergfeld, D. V. Belsito, R. A. Hill, C. D. Klaassen, D. C. Liebler, J. G. Marks, R. C. Shank, T. J. Slaga, P. W. Snyder, L. J. Gill and B. Heldreth, *Int. J. Toxicol.*, 2019, **38**, 68–228.

121 R. M. Giner, J. L. Ríos and S. Máñez, *Antioxidants*, 2022, **11**, 343.

122 N. J. Walton, M. J. Mayer and A. Narbad, *Phytochemistry*, 2003, **63**, 505–515.

123 S. Marimuthu, K. Krishnamurthy, K. Karunanandham and M. Ponnusamy, *African J. Microbiol. Res.*, 2014, **8**, 2486–2491.

124 I. Itabaiana Junior, M. Avelar Do Nascimento, R. O. M. A. De Souza, A. Dufour and R. Wojcieszak, *Green Chem.*, 2020, **22**, 5859–5880.

125 Z. Ahamed, J. kyu Seo, J. U. Eom and H. S. Yang, *LWT*, 2023, **188**, 115374.

126 H. Zhang, Z. Wang and O. Liu, *J. Pharm. Anal.*, 2015, **15**, 224.

127 S. Purohit, M. K. Bohra and R. Jain, *Appl. Biochem. Biotechnol.*, 2023, **195**, 2235–2251.

128 J. X. Jia, K. M. Wasan and J. Pharm, *Pharm. Sci.*, 2008, **11**, 45–62.

129 K. Paramasivan and S. Mutturi, *World J. Microbiol. Biotechnol.*, 2022, **38**, 91.

130 X. Yu, C. Zhang, H. Wang, Y. Li, Y. Kang and K. Yang, *ACS Omega*, 2023, **8**, 20823–20833.

131 A. K. Maldhure, *Int. J. Pharma Bio Sci.*, 2015, **6**, 810–815.

132 L. I. Fajimi and B. O. Oboirien, *J. Mater. Cycles Waste Manag.*, 2023, **25**, 3462–3475.

133 B. Alawa and S. Chakma, *Environ. Sci. Pollut. Res.*, 2023, **30**, 64006–64024.

134 S. M. Selvam, P. Balasubramanian, M. Chintala and L. K. S. Gujjala, *Biomass Convers. Biorefin.*, 2025, **15**, 14229–14239.

135 B. Behera, D. Laavanya and P. Balasubramanian, *Bioresour. Technol.*, 2022, **346**, 126559.

136 J. N. Ullas Krishnan, S. Poddar, T. Sriharsha, A. K. Maroli and J. Sarat Chandra Babu, *Indian Chem. Eng.*, 2024, **64**, 393–402.

137 D. Varshney and P. Mandade, *Sustain. Prod. Consum.*, 2019, **18**, 96–114.